From AGB Stars to Planetary Nebula

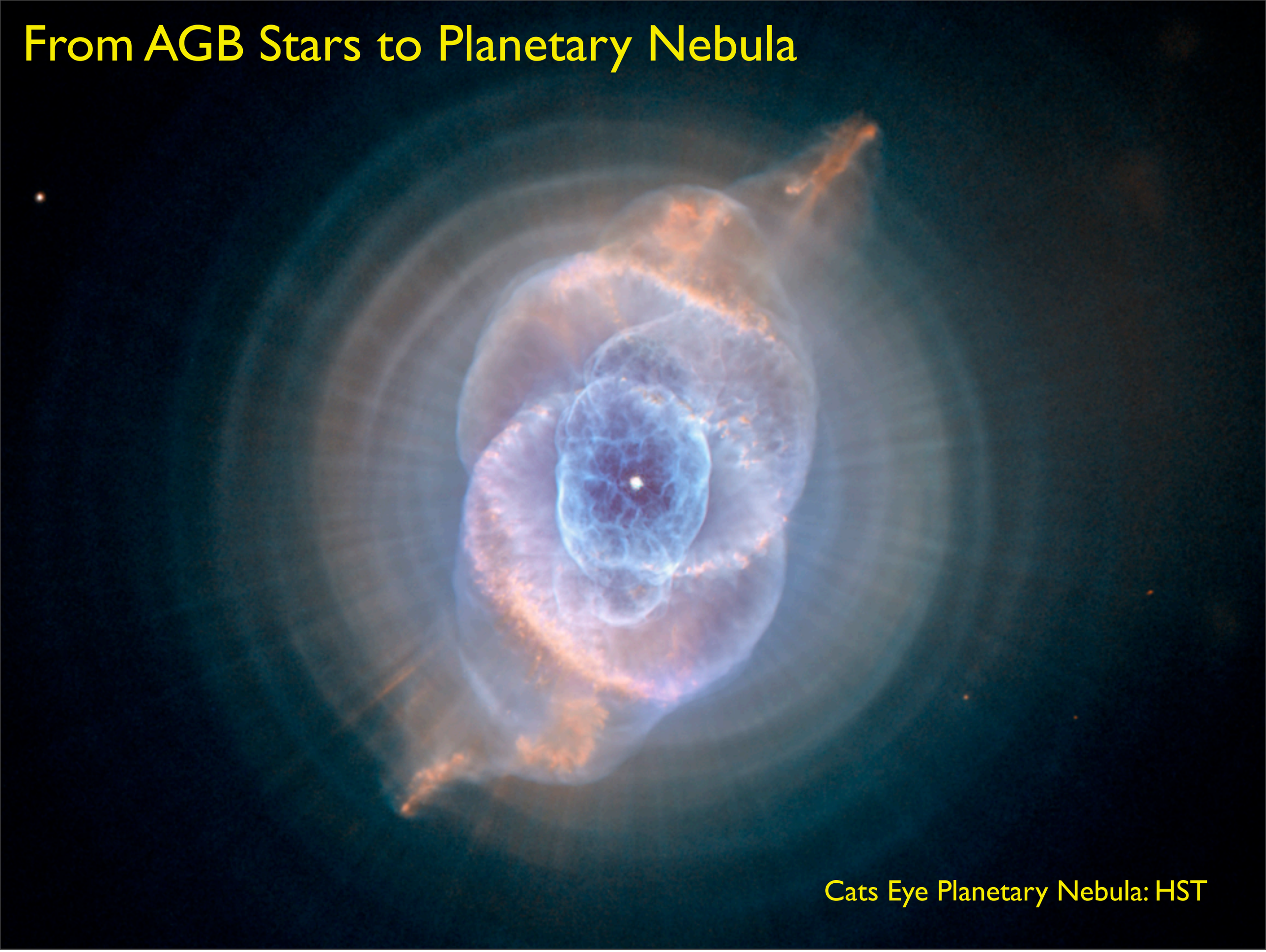

Cats Eye Planetary Nebula: HST

AGB Stars

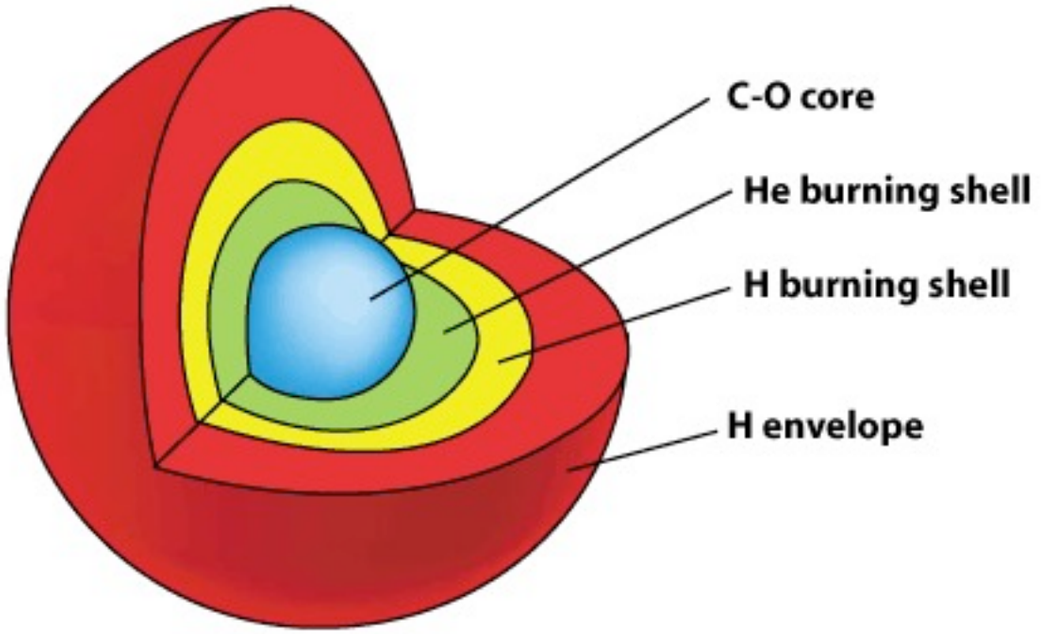

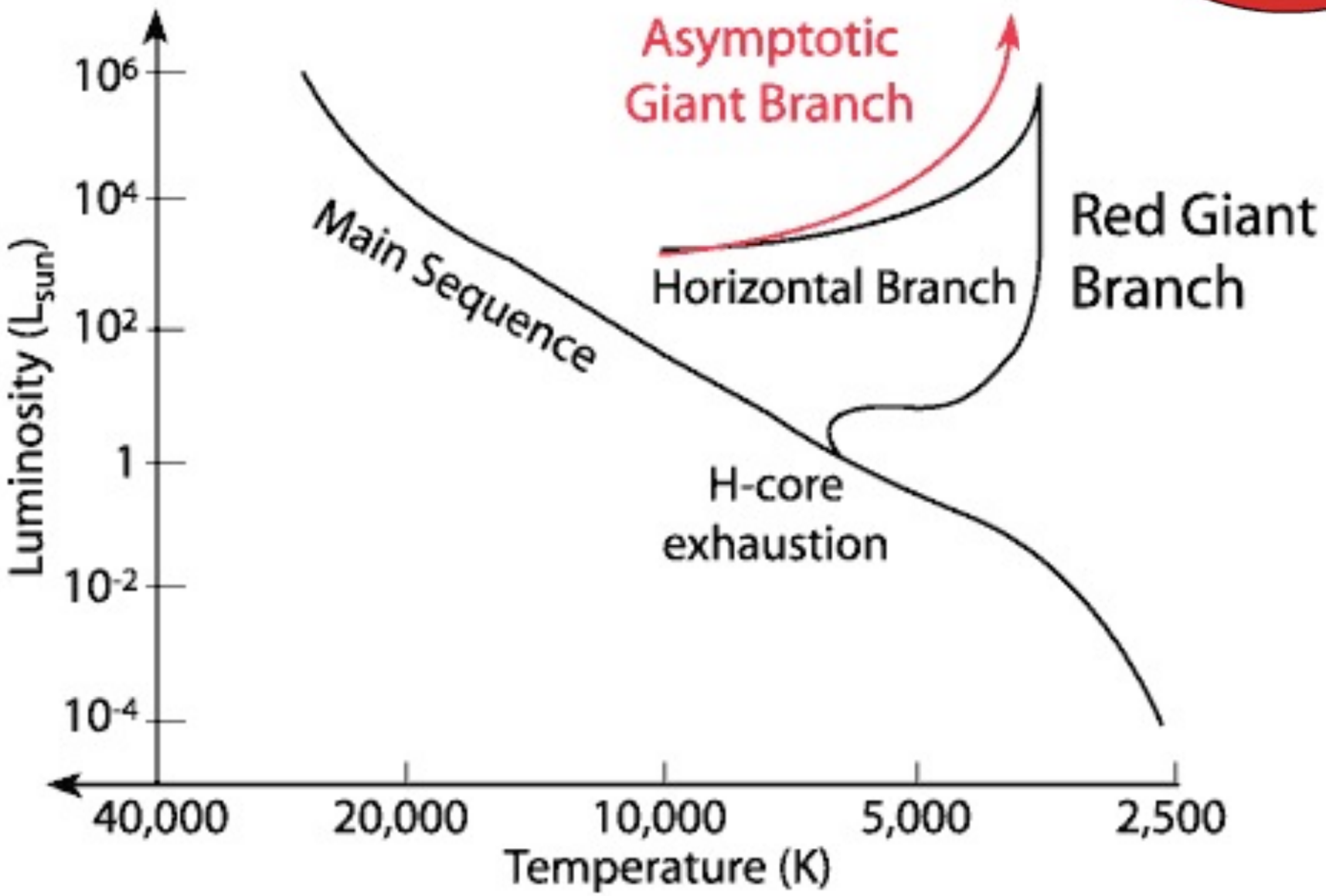

NOAO

H -> He
in convective
region

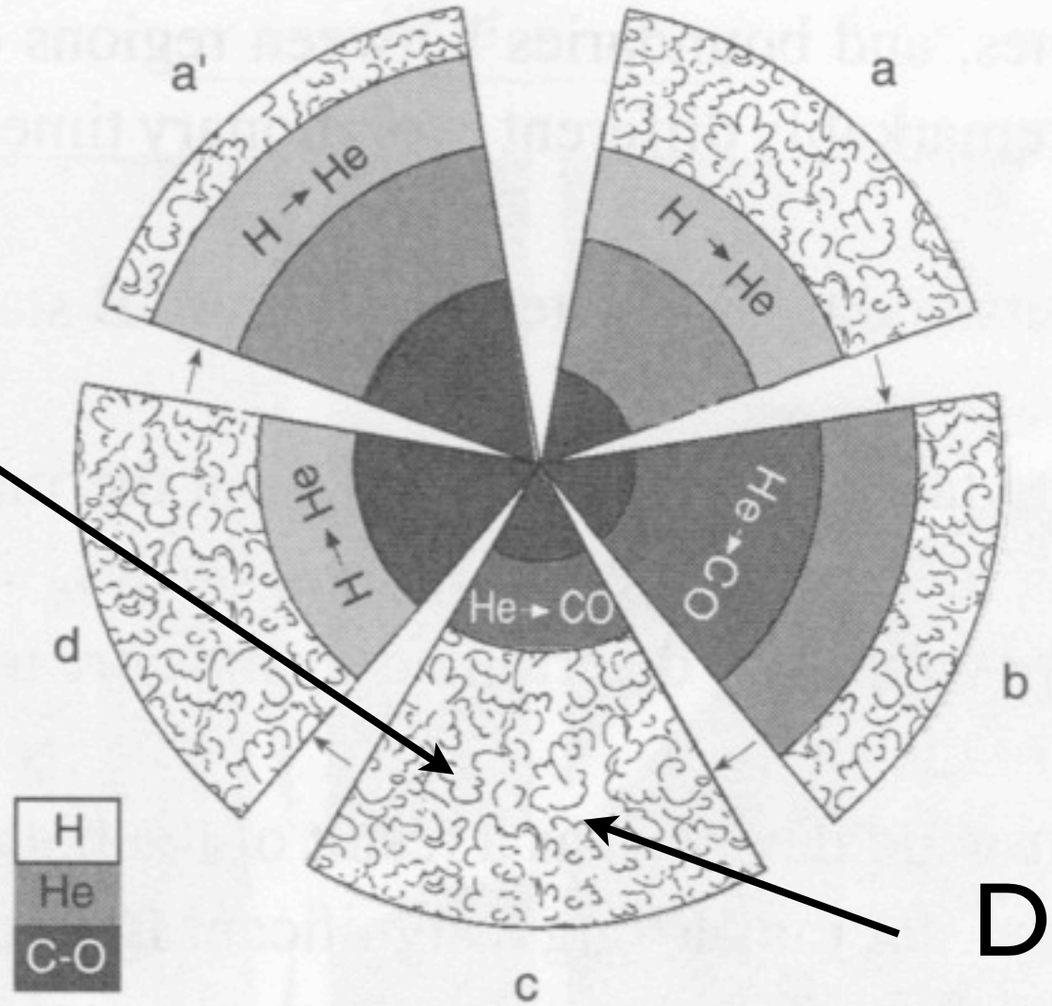

Dredge Up

Figure 8.10 Sketch of the progress of a thermal pulse cycle through its different stages (not in scale). Hydrogen is burning during stages a and d, while helium is burning during stages b and c. When, in stage c, the outer convective zone extends inward beyond the helium shell burning boundary, hydrogen and helium burning products are mixed into the envelope and dredged up to the surface. Stage a′ is the same as a, except that the carbon-oxygen core has grown at the expense of the envelope.

Prialnik

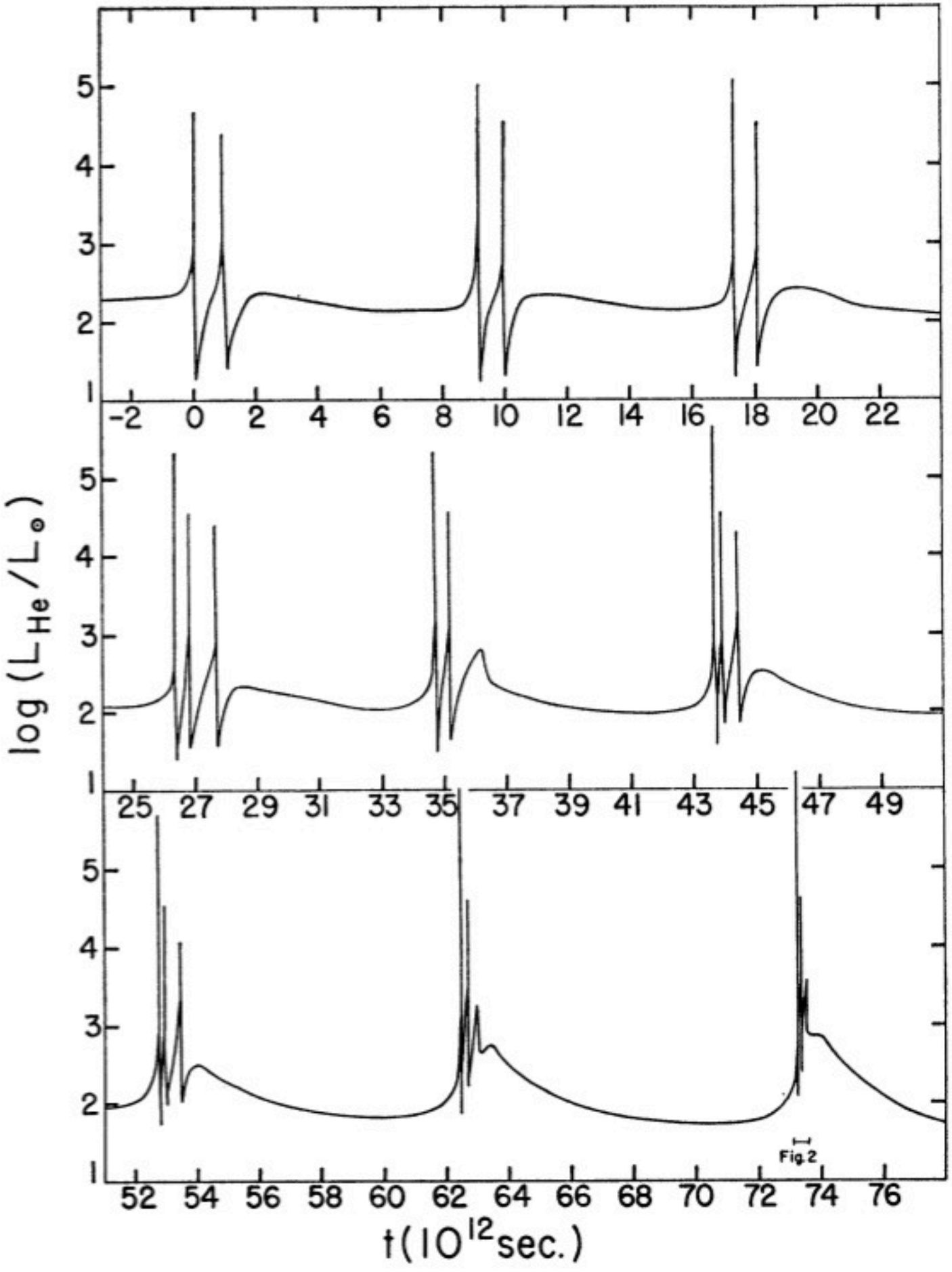

AGB stars pulsing

Schwarzchild & Harm (1967)

The 9th Cycle

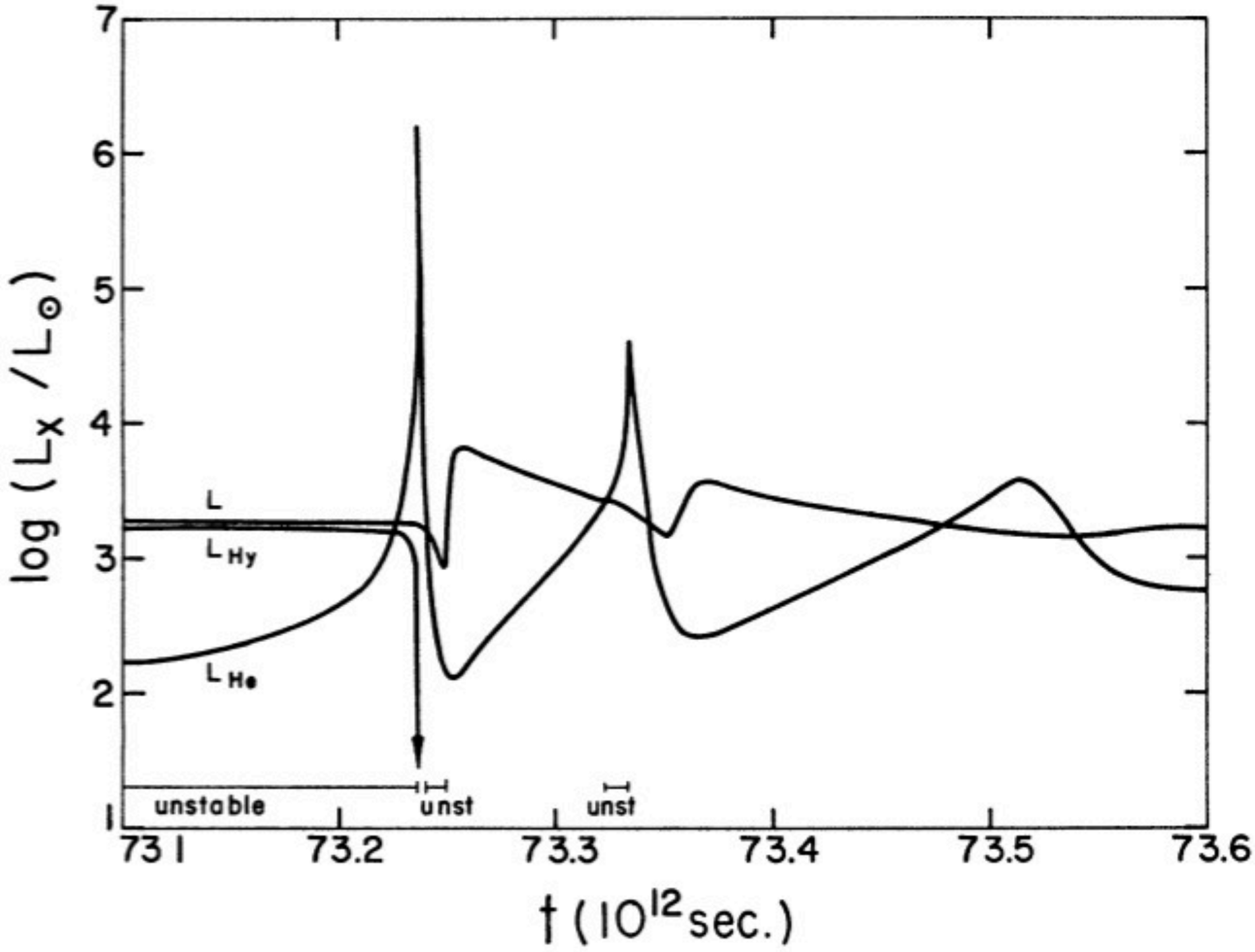

Schwarzchild & Harm (1967)

Dredge-Ups

- First dredge up: generation of convective zone formation on Red Giant Branch (brings up gas processed by H burning)
- Second dredge up: after the Helium burning ceases (CNO products from Hydrogen shell burning)
- Third dredge up: during AGB pulses: stuff from Helium burning and S-process (and maybe carbon burning for intermediate mass stars)

Winds and Superwinds

Consider a wind driven by photon pressure

$$\dot{M} v_{esc} = \phi \frac{L}{c}$$

where ϕ is the fraction of photons absorbed. Given that $v_{esc}^2 = 2GM/R$. Then

$$\dot{M} = \phi \frac{v_{esc}}{c} \frac{LR}{2GM}$$

Empirically, Dieter and Reimers found that:

$$\dot{M} \approx 10^{-13} \frac{L}{L_\odot} \frac{R}{R_\odot} \frac{M_\odot}{M} M_\odot \; yr^{-1}$$

A much higher mass loss rate would be a Superwind

Mira (the wonder) aka Omicron Ceti

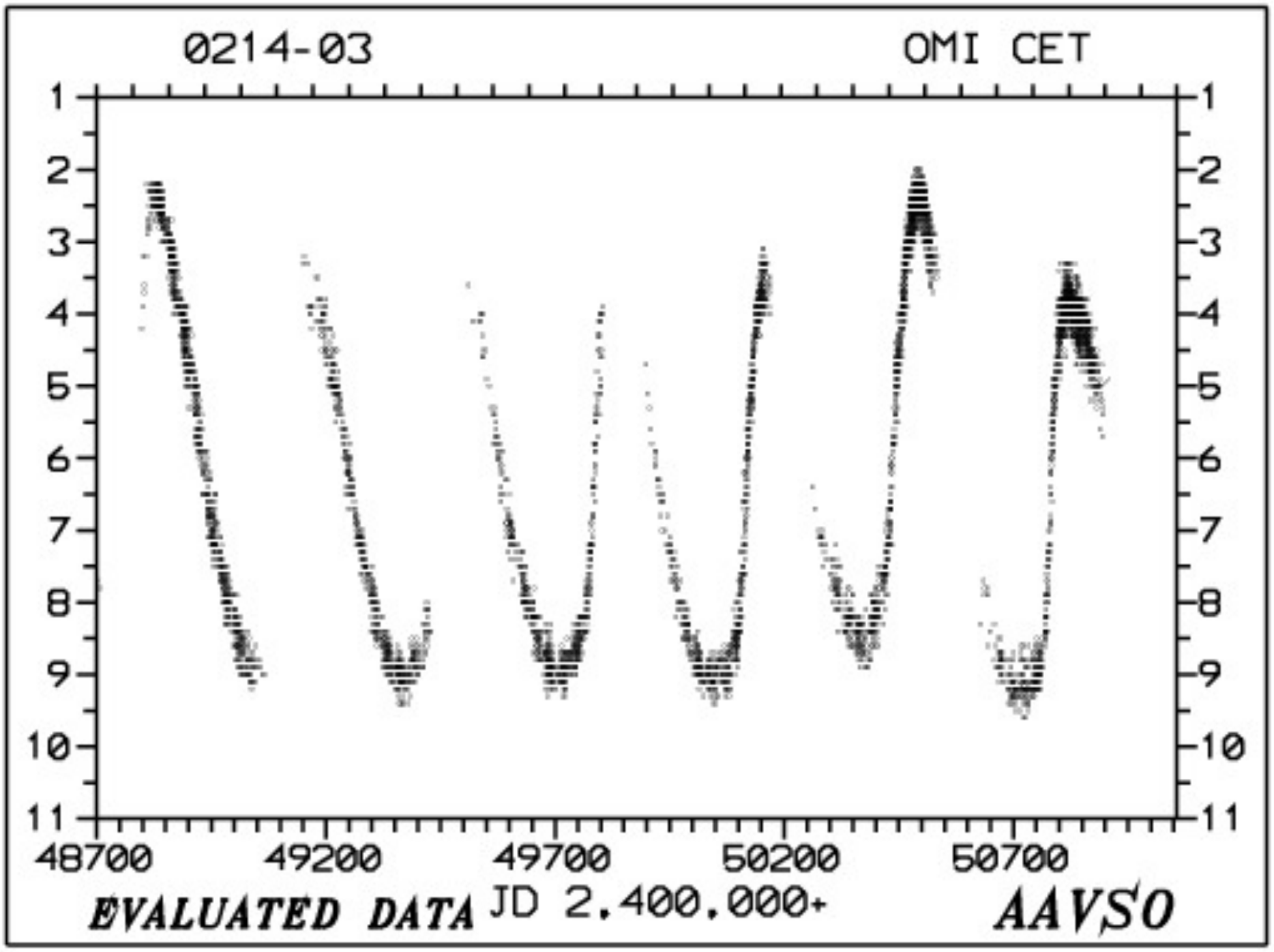

These pulsations are much more rapid than the thermal pulses (which take 10,000s of years)

http://www.aavso.org/vsots_mira

Mira Variables

The Mira variables are named after the prototype Mira.

Discovered as a variable in 1596.

Mira is a 1.5 solar mass star in an AGB phase.

Distance: 107 pc

Radius: ~ 400 Rsun

Luminosity ~ 9000 Lsun.

Periods 150 to 1000 days

Mdot = 3 x 10^{-7} Msun yr^{-1}
v_w = 5 kms^{-1}

Mira Variables as a class are cool (3000 K), big 200-300 solar radii, and luminous: ~4000 Lsun.

Often have spectral class M, S (zirconian oxides and C~O) or C (strong carbon lines

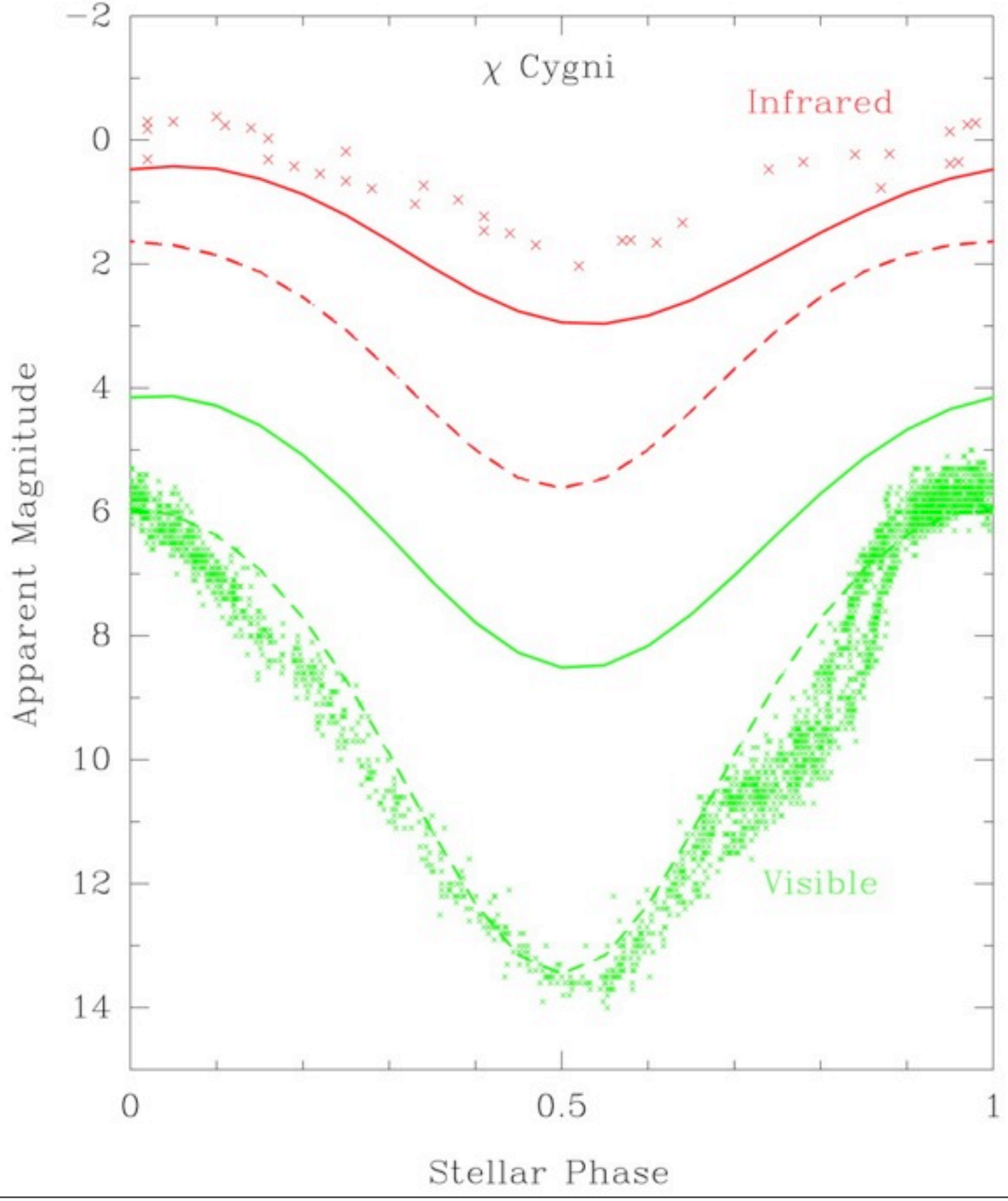

Mira Variables and Sunscreen

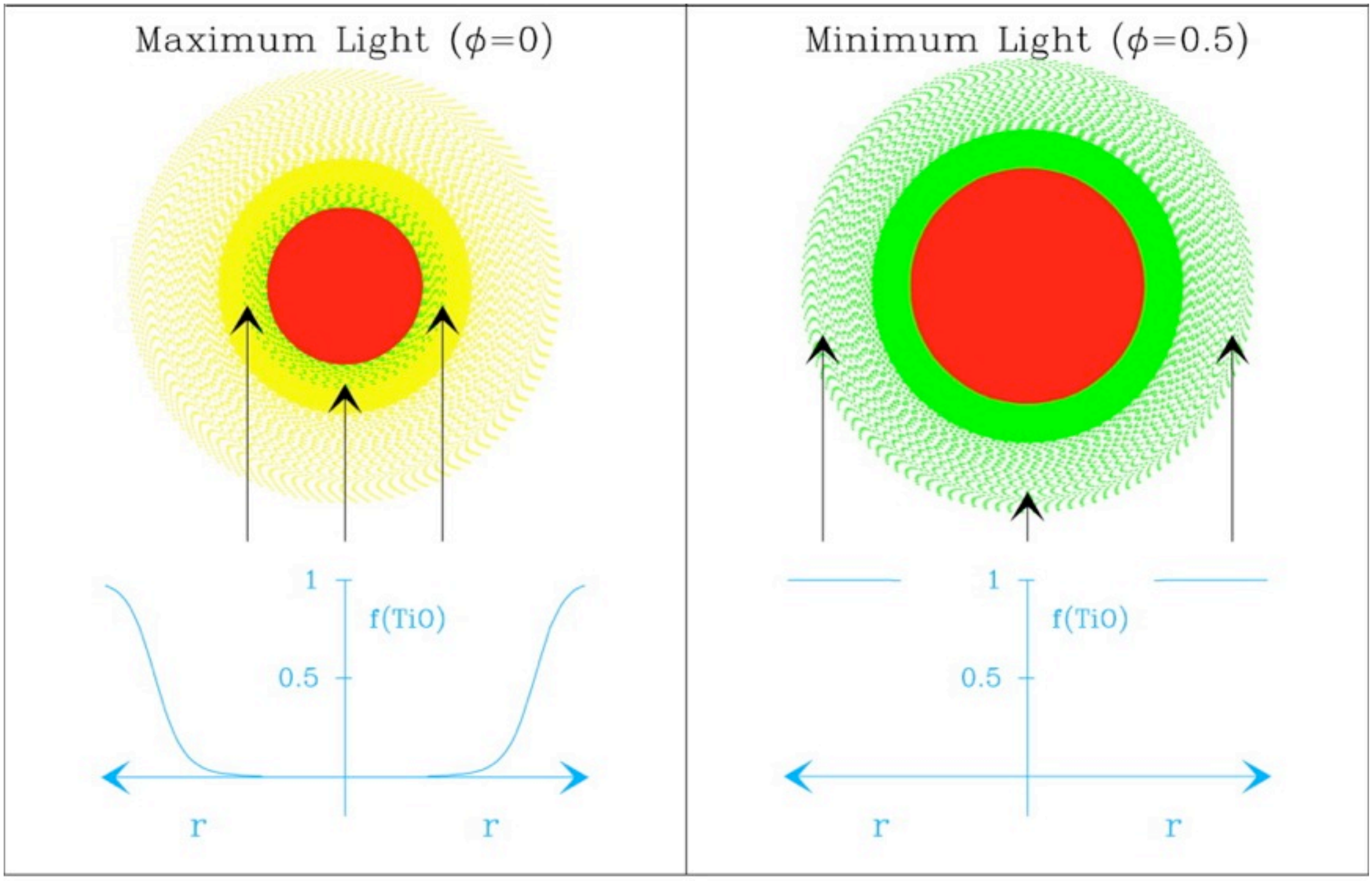

Large changes in visible brightness may be the result of TiO (sunblock) forming in the outer atmospheres.

Reid & Goldston 2002

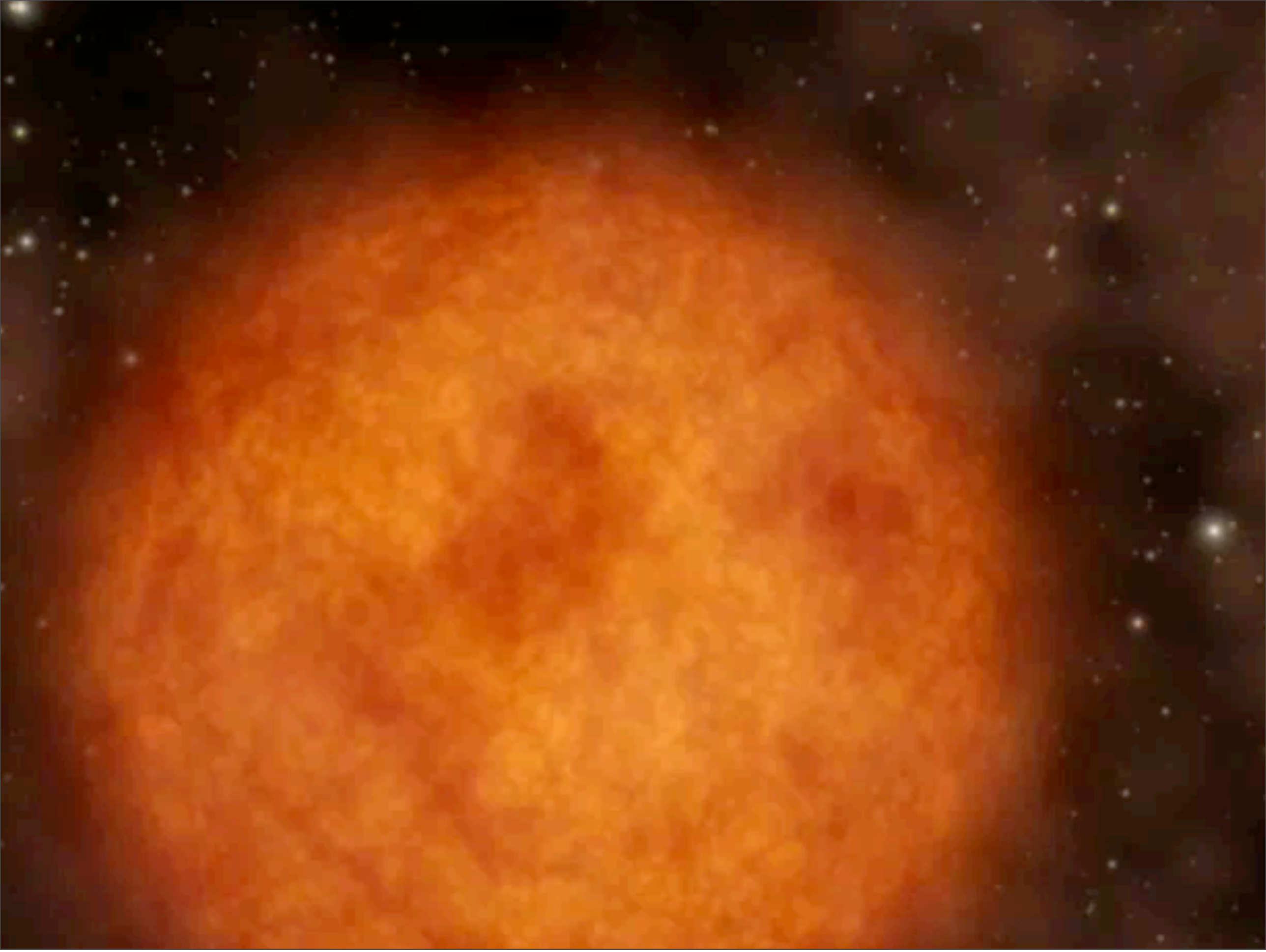

Mira's bow shock and tail (Martin et al. 2007)

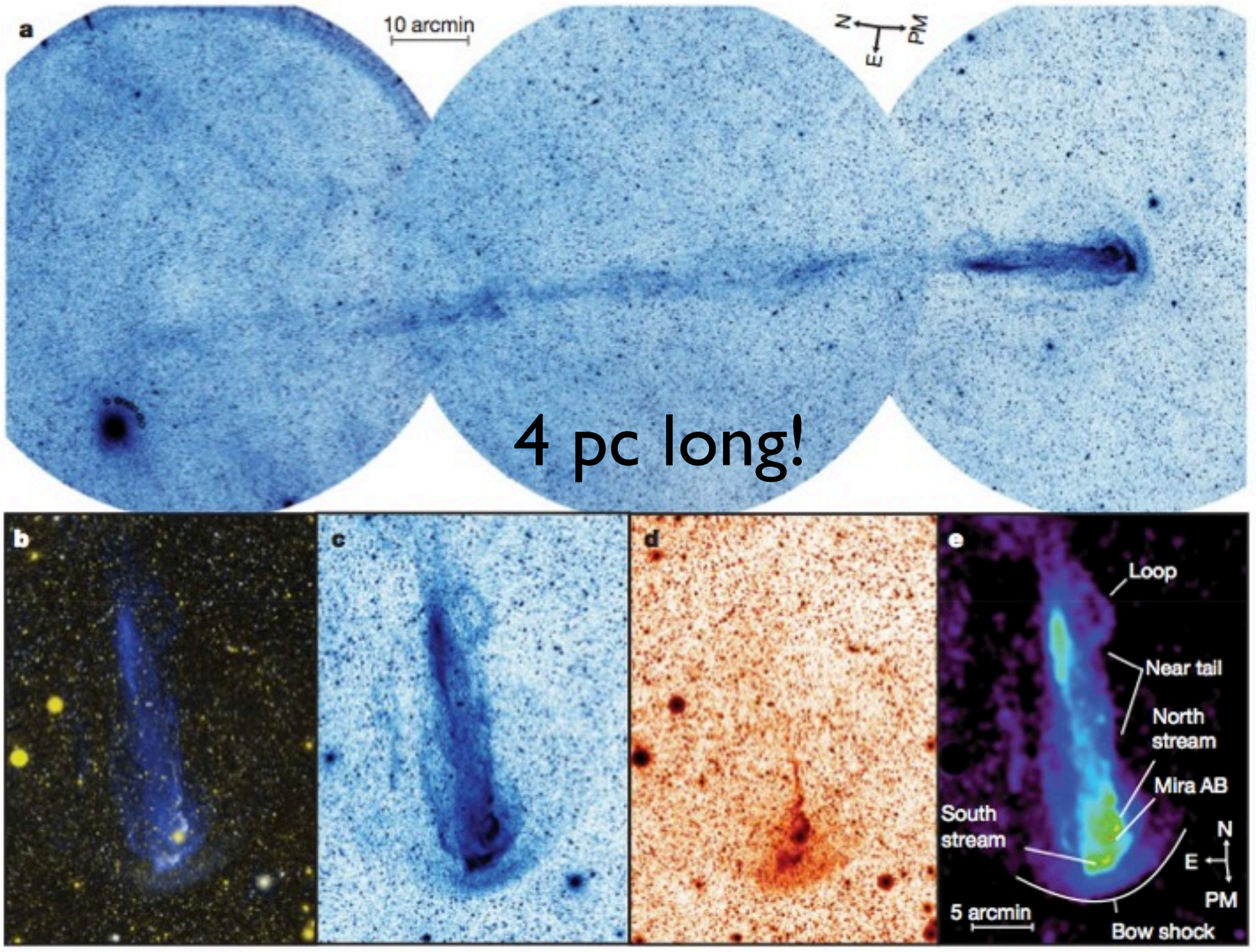

Figure 1 | Ultraviolet imaging of the Mira tail and bow shock. **a**, The far-ultraviolet (effective wavelength $\lambda_{eff} = 151.6$ nm; full-width at half-maximum, FWHM = 25.6 nm) mosaic of the Mira AB tail and bow shock. The data have been histogram equalized. The co-added mosaic consists of 31 observations covering 3 pointings with a total exposure time of 8.9, 11.2 and 11.5 ks (left to right). The images were taken between 18 November and 15 December 2006. The rectangular region is 2.7 × 1.1 degrees. The orientation (N, E) and measured proper motion (PM) vectors are indicated. The observed position angle of the tail is 194 degrees, in agreement with the observed proper motion vector once solar motion is accounted for. **b**, Energy-scaled colour composite image. Far ultraviolet is blue; near ultraviolet ($\lambda_{eff} = 226.7$ nm; FWHM = 73.0 nm) is red; the average of the two ultraviolet bands is green. The region is 26 × 36 arcmin with an exposure time of 11.5 ks. North is up and east is left. The images were taken on 18–19 November 2006. **c**, **d**, The histogram-equalized far-ultraviolet (**c**) and near-ultraviolet (**d**) images covering the same physical region as **b**. There is a weak near-ultraviolet contribution to the bow shock and a complete lack of near-ultraviolet emission in the near-tail region. Each image has been boxcar-smoothed by 2 pixels (3 arcsec). **e**, This far-ultraviolet image has been enhanced by point source subtraction and adaptive smoothing.

Mira is a Binary (separation ~0.5” or ~50 AU)

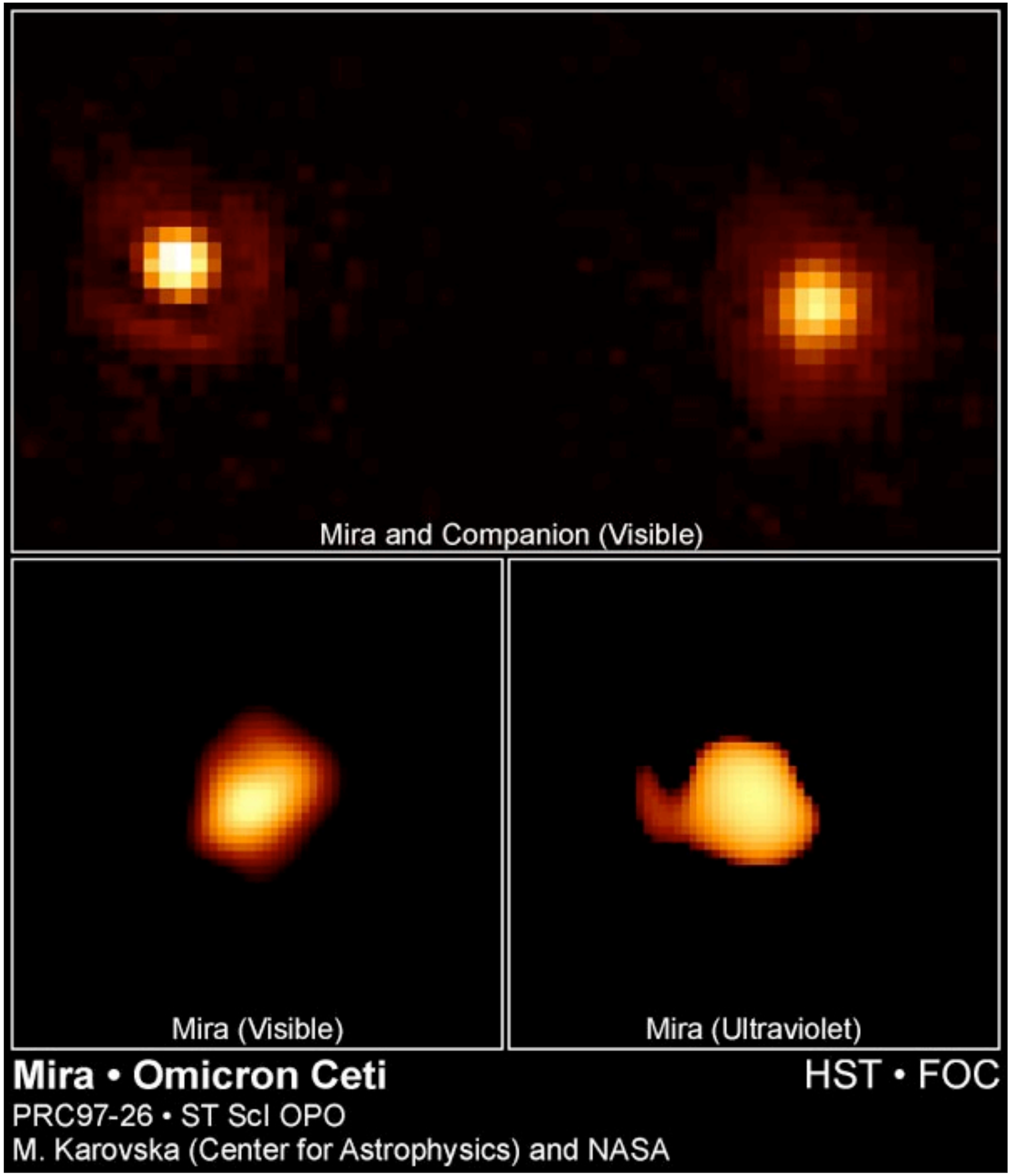

A Jet from Mira

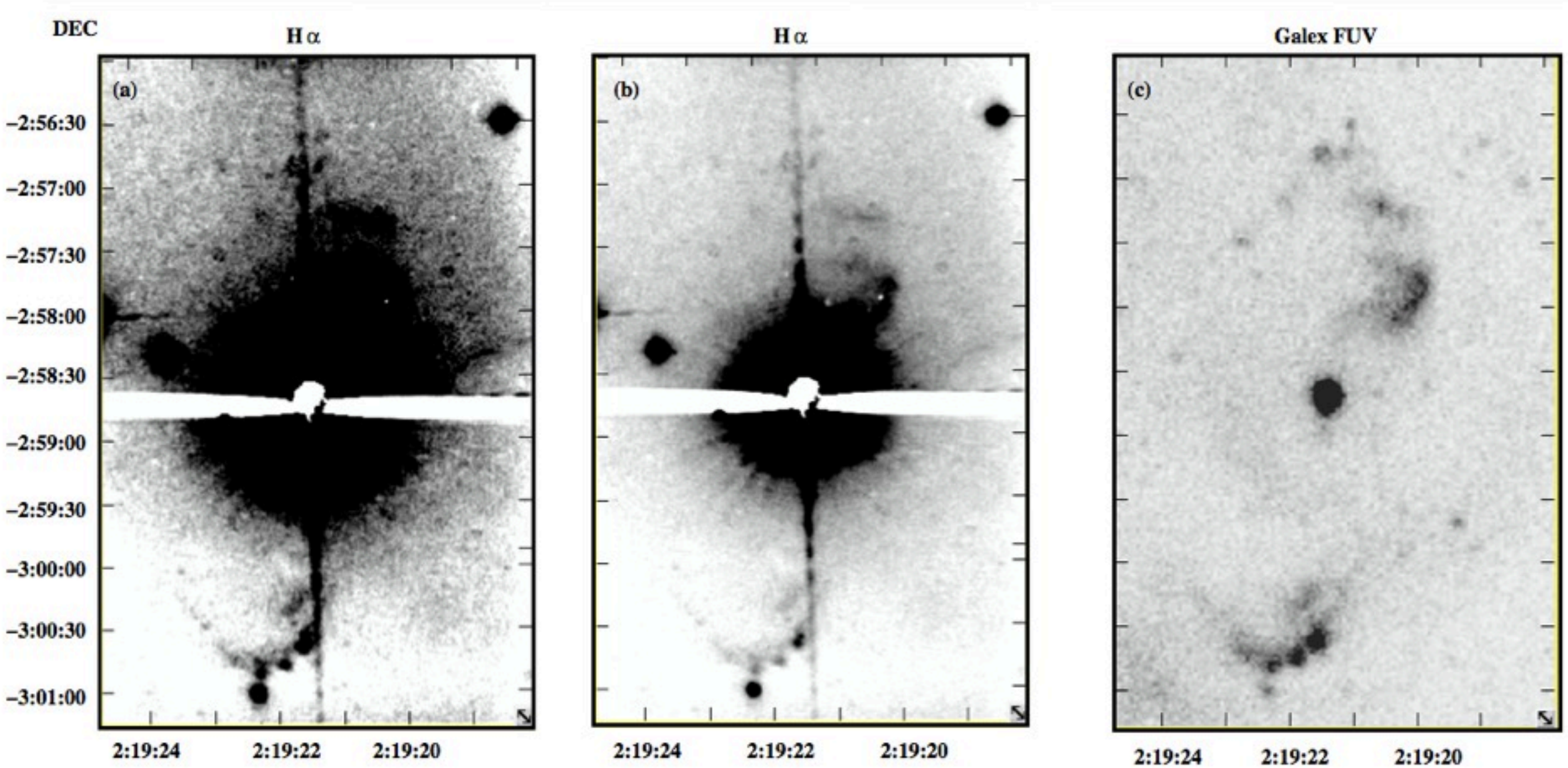

OH/IR Stars

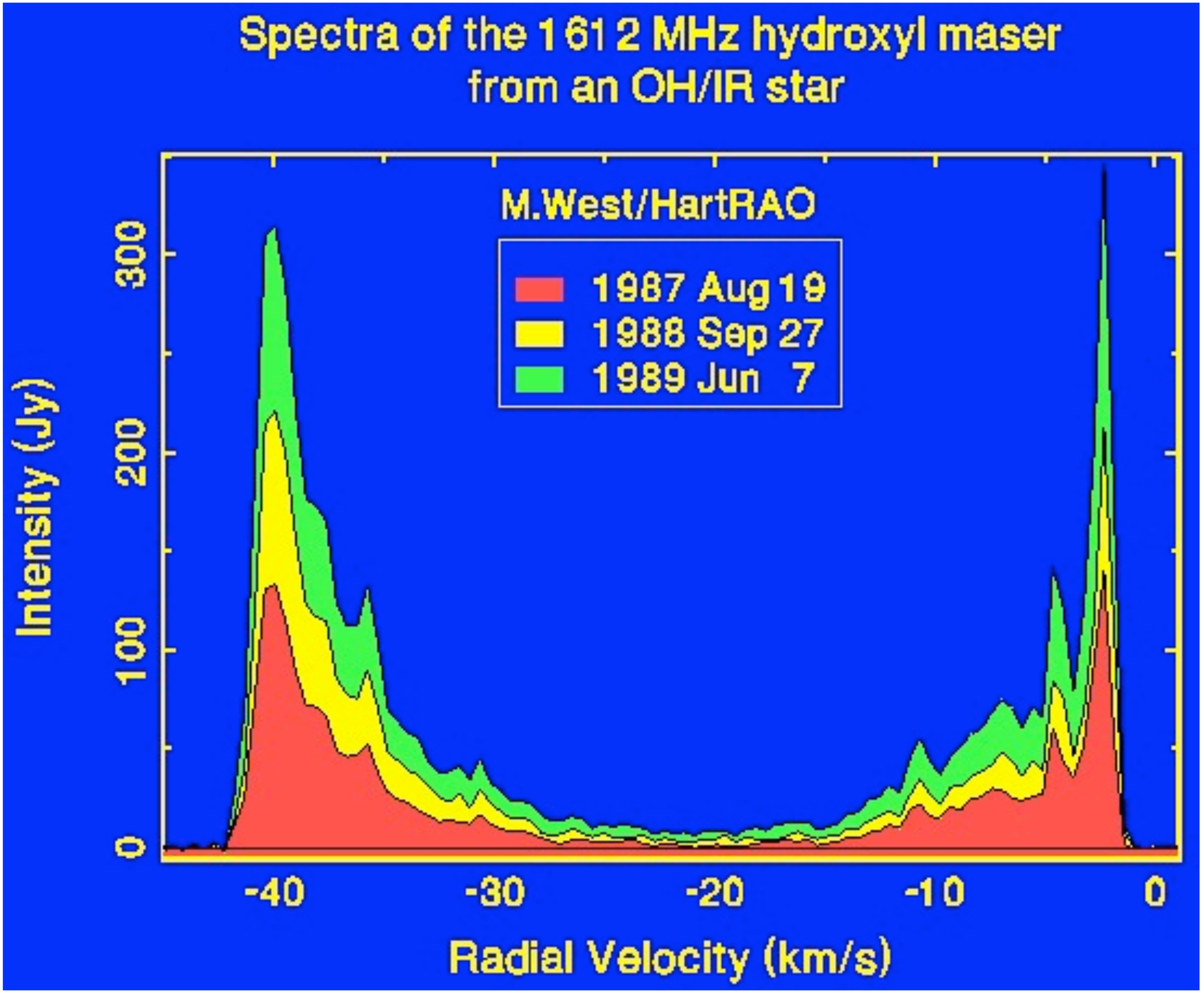
Spectra of the 1612 MHz hydroxyl maser
from an OH/IR star
M.West/HartRAO
1987 Aug 19
1988 Sep 27
1989 Jun 7
Intensity (Jy)
0
100
200
300
-40
-30
-20
-10
0
Radial Velocity (km/s)

OH/IR Stars

Engels: ESO Messenger

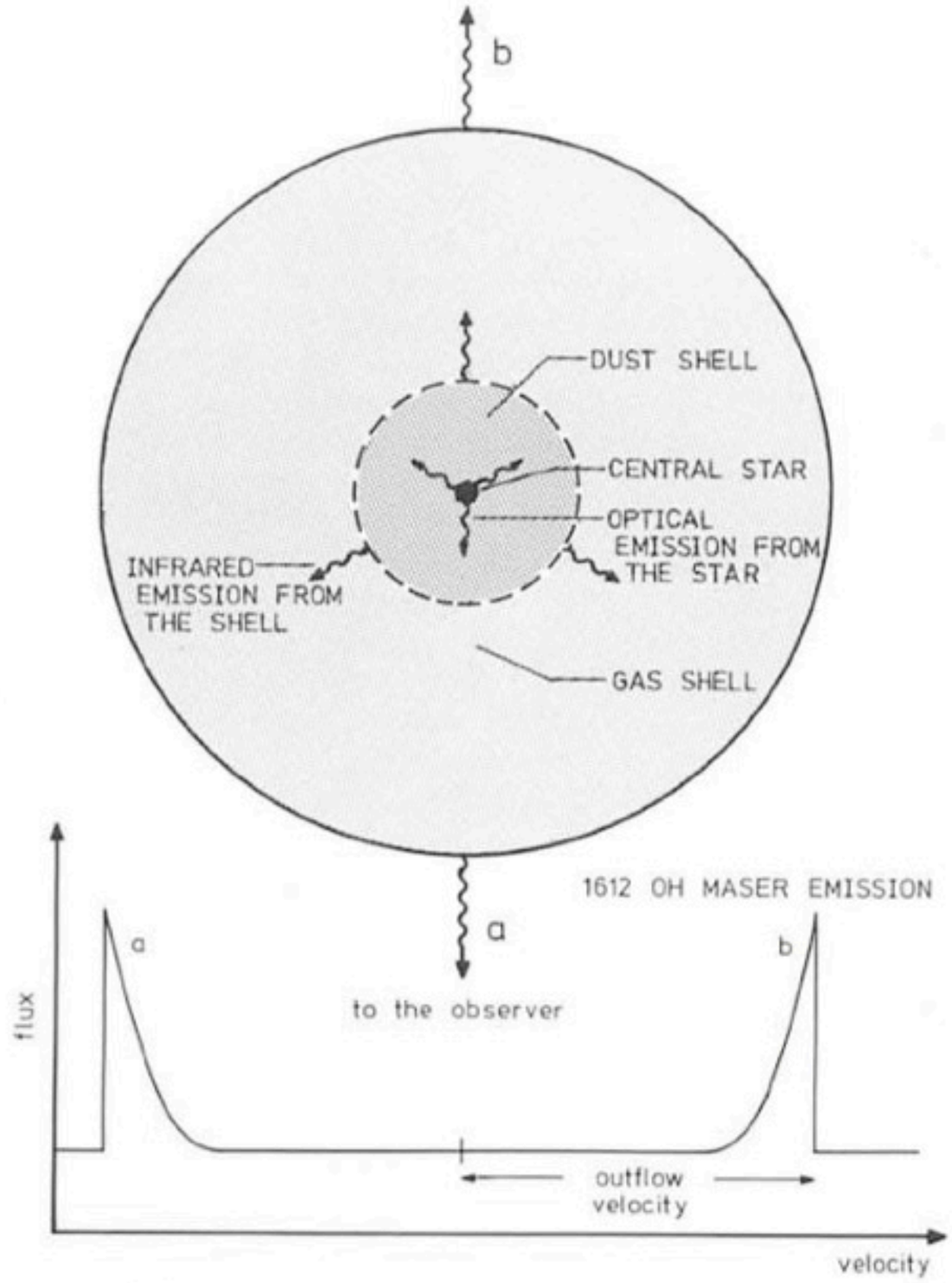

Fig. 1: *Schematic picture of an OH/IR star (above). The central star is surrounded by an expanding circumstellar dust and gas shell, which absorbs the optical emission from the star and reemits the energy in the infrared. The OH masers are located in the outer parts of the shell. At earth the OH maser emission is observed in two velocity groups (below). The low velocity component (a) comes from the front whereas the high velocity feature (b) comes from the back side of the shell.*

Dust Formation

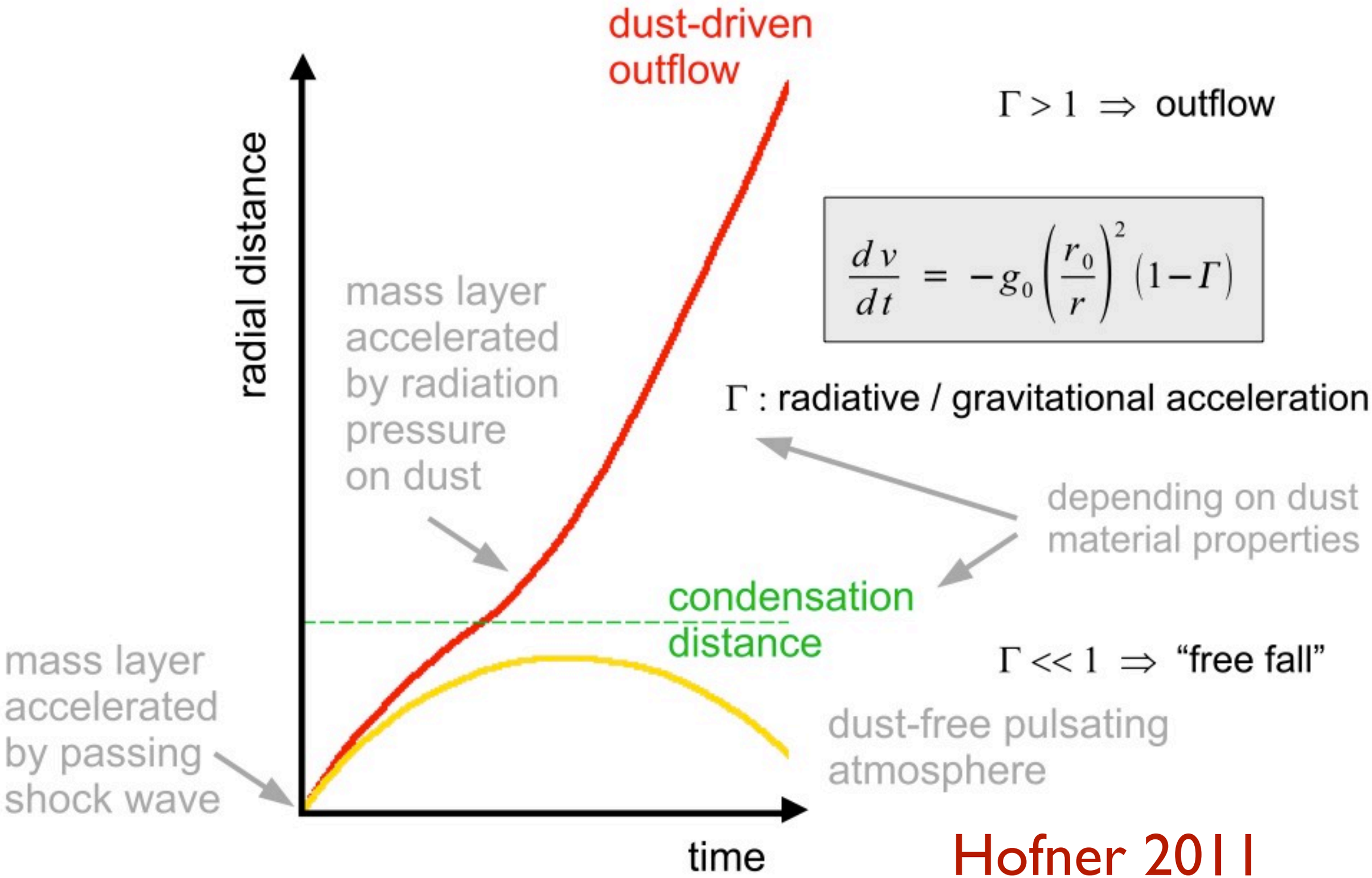

Hofner 2011

OH/IR Stars

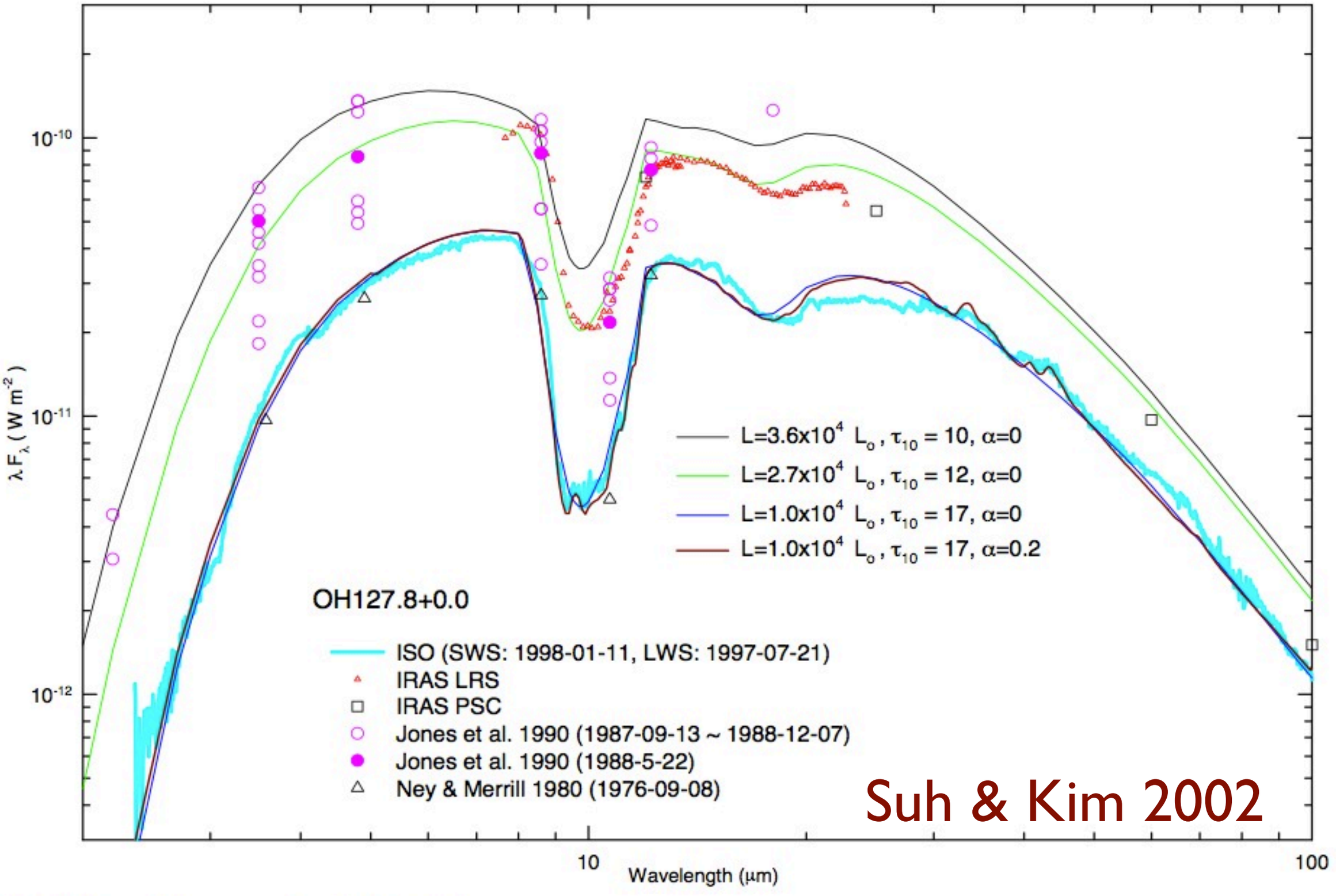

Suh & Kim 2002

Fig. 3. SEDs at different phases for OH127.8+0.0.

Measuring Mass Loss from AGB Stars

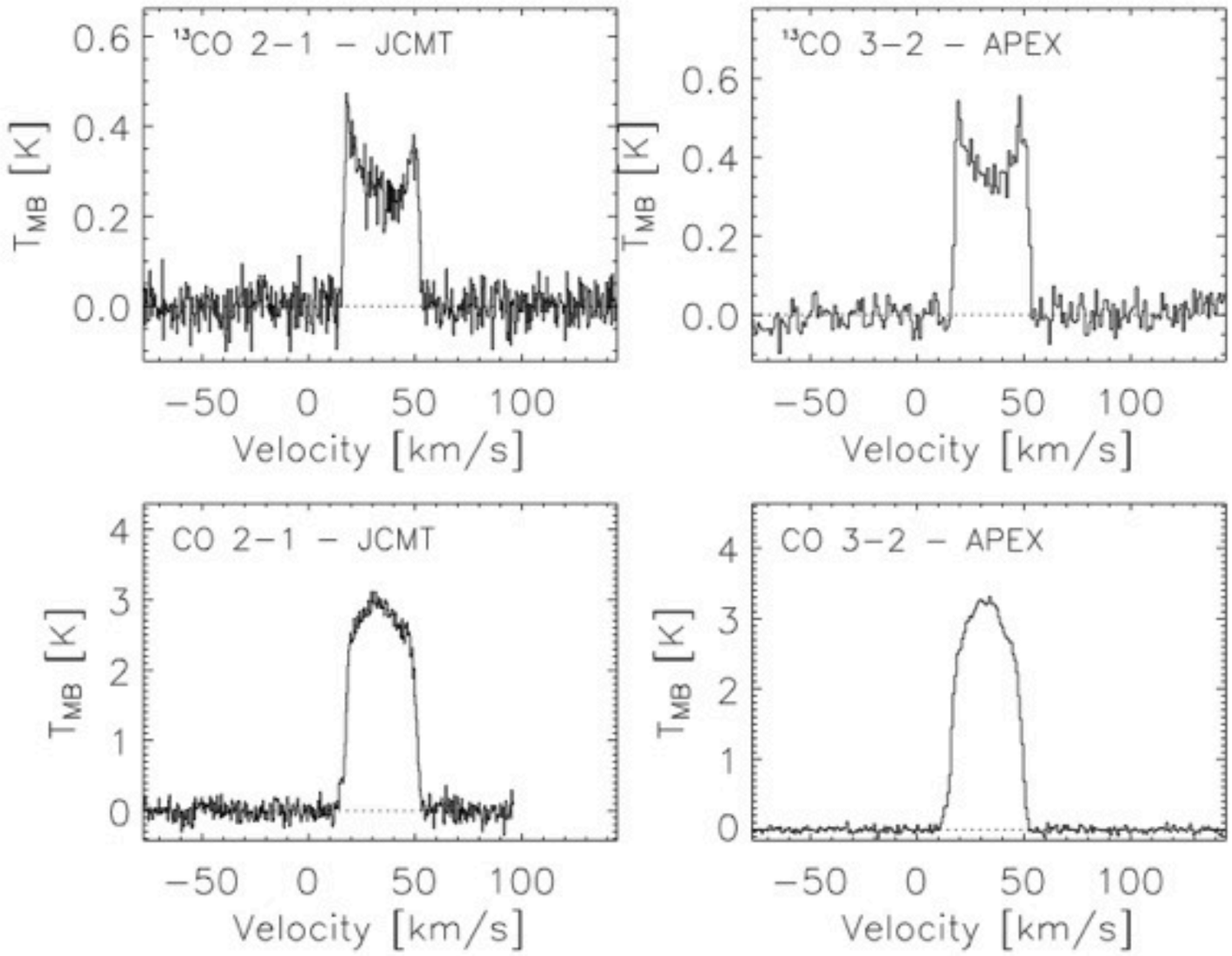

Fig. 1. ^{12}CO and ^{13}CO data of IK Tau, obtained with JCMT and APEX. It is clear from the graphs that the ^{12}CO lines are more parabolic in shape than the ^{13}CO lines. This effect is caused by the lower abundance of ^{13}CO, leading to optically thinner line profiles.

De Beck et al 2011

Measuring Mass Loss from AGB Stars

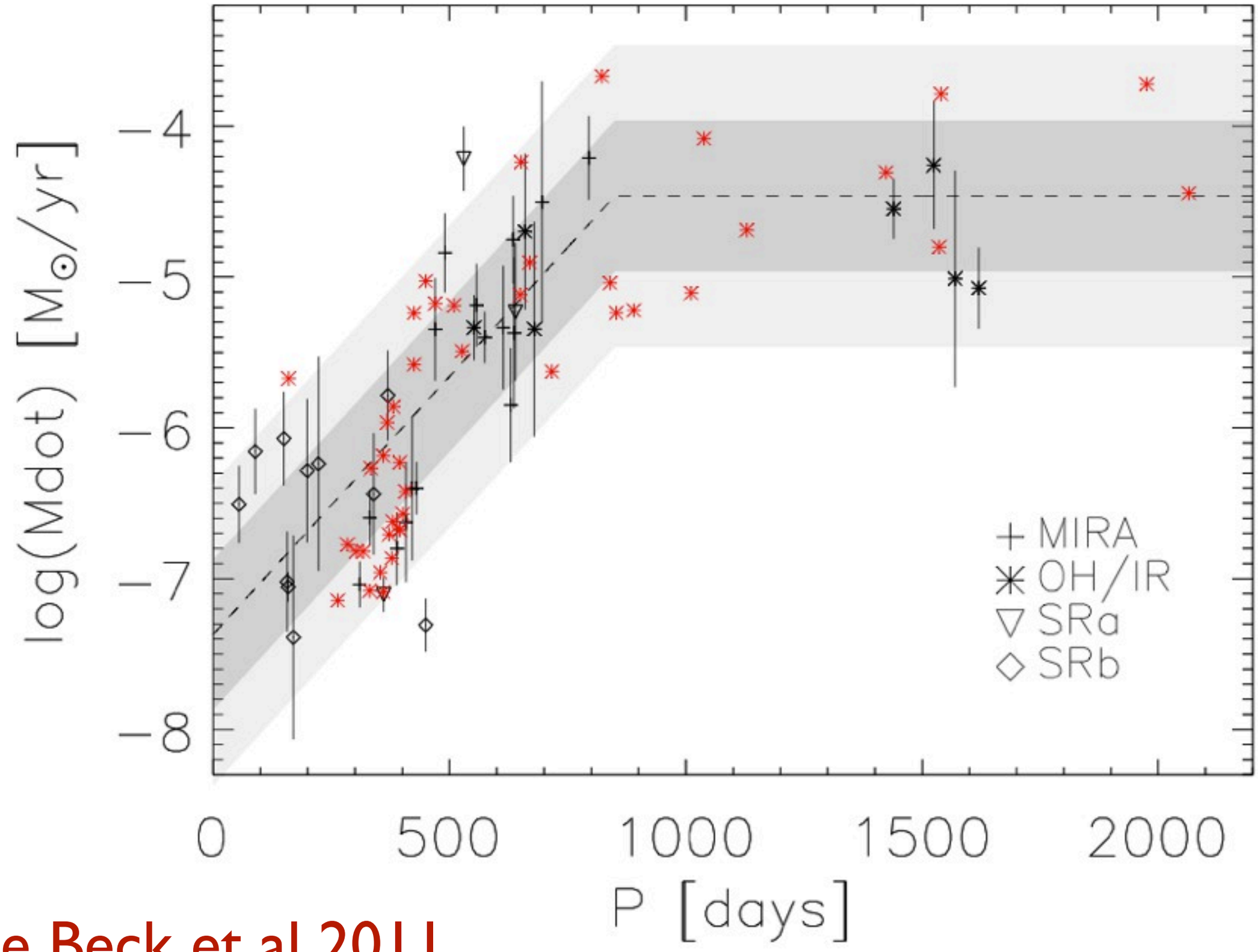

De Beck et al 2011

Measuring Mass Loss from AGB Stars

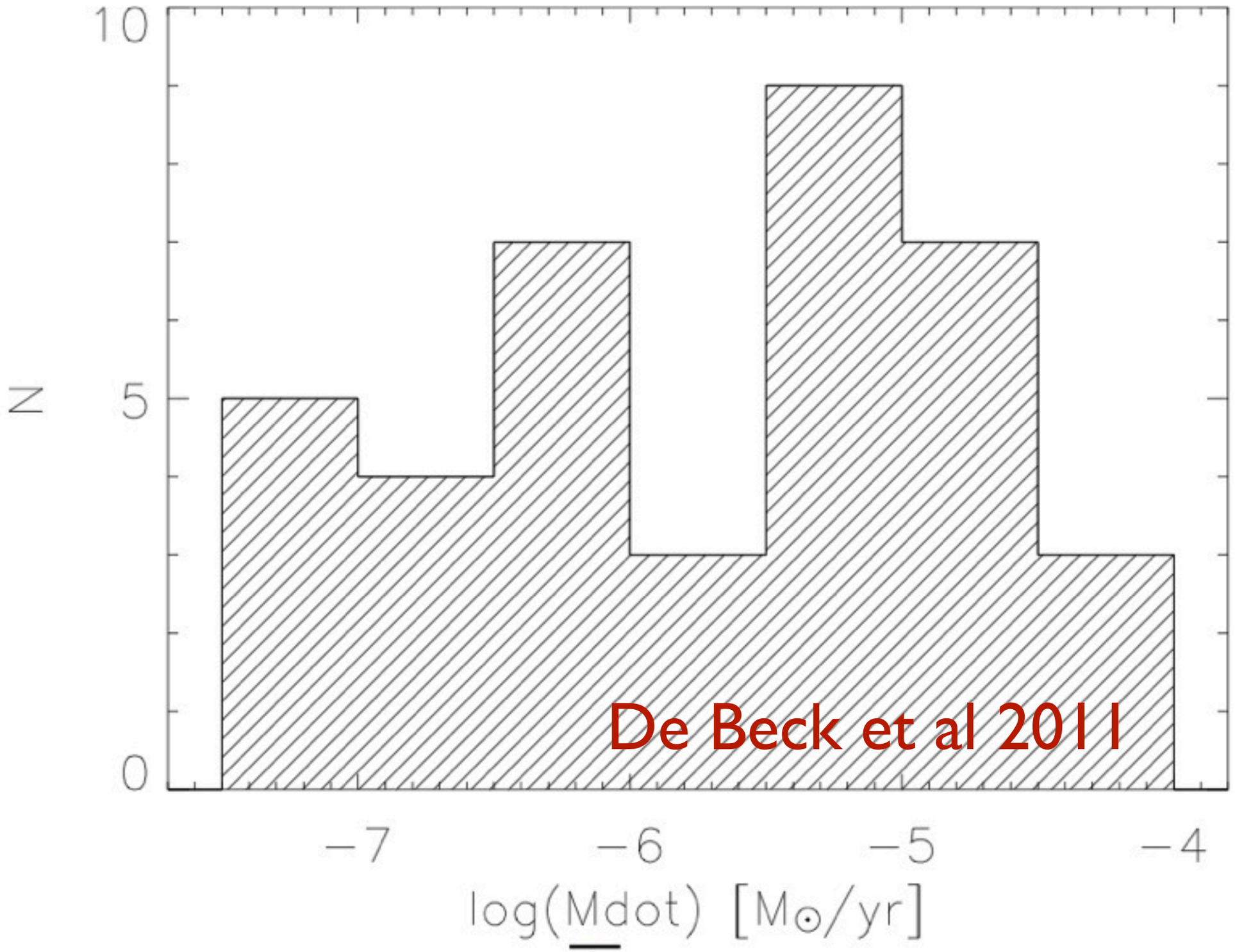

(c) Histogram of the $\dot{M}$-values of all AGB stars.

Planetary Nebula are not spherically symmetric. The are often elliptical. They show jets and other structures. What causes this asymmetry?

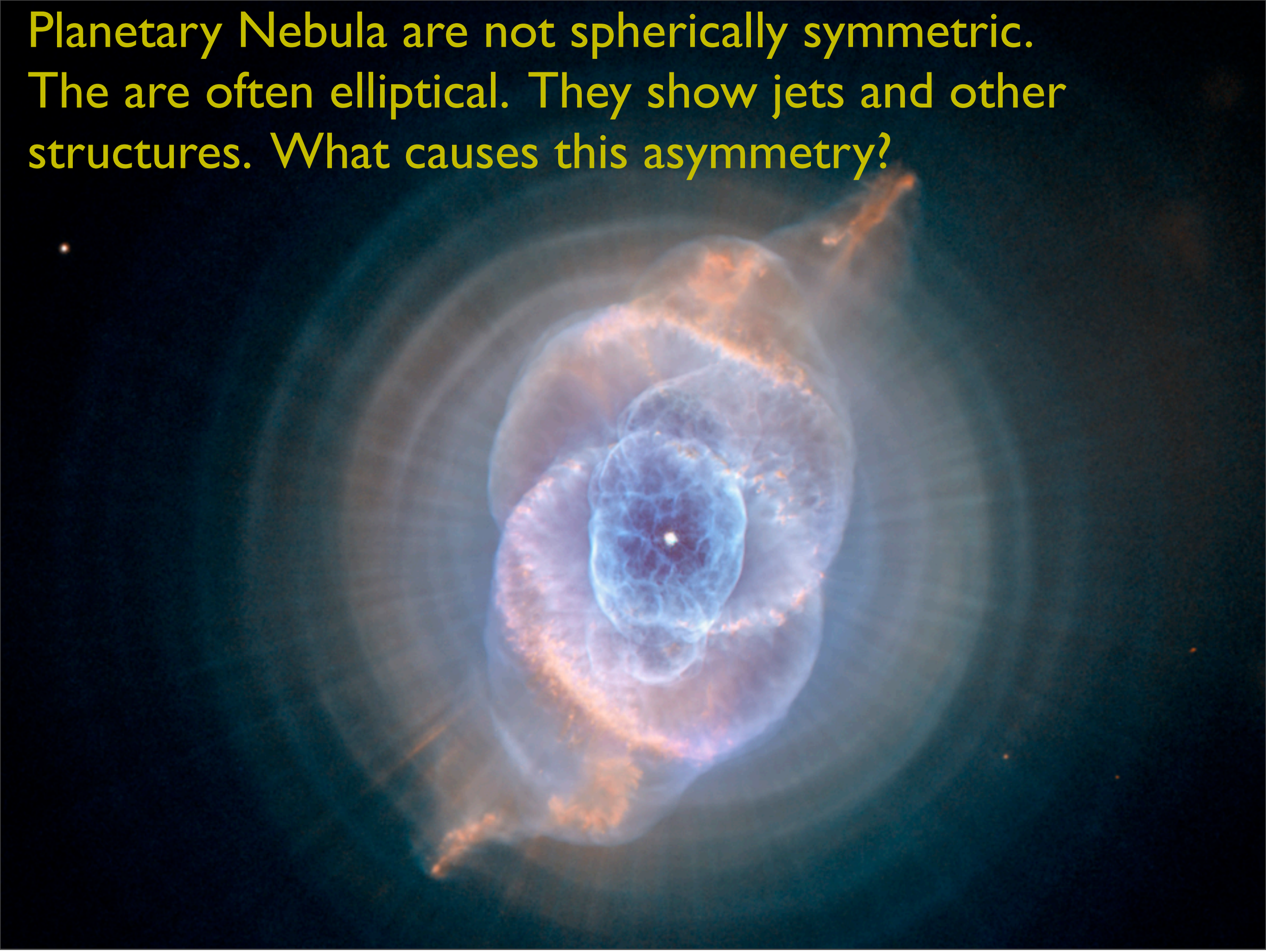

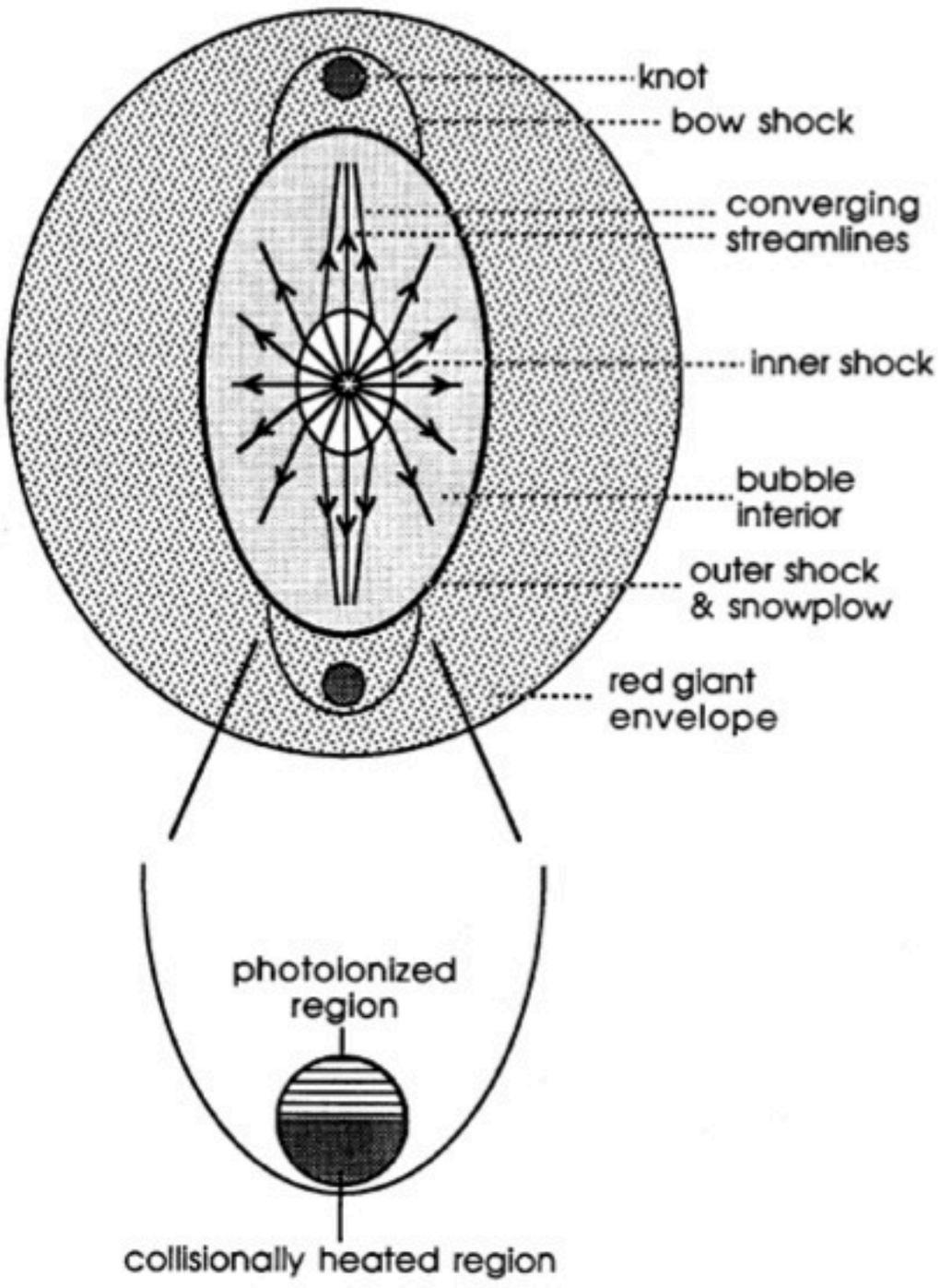

FIG. 9. Sketch of the spindle model. Top: the relative locations of the RGE and the central star, the latter surrounded by its reverse shock and the outer shock. Bottom: a knot that has formed in the collimated axial flow, preceded by its bow shock. The upstream side of the knot is collisionally heated: possibly the downstream side shows some photoionization.

Fast and Slow Winds

Slow wind 10^{-4} - 10^{-5} Msun yr^{-1}
V = 10 km s^{-1}
Fast wind 10^{-7} - 10^{-8} Msun yr^{-1}
V = 2000 km s^{-1}

Balick et al. 1987

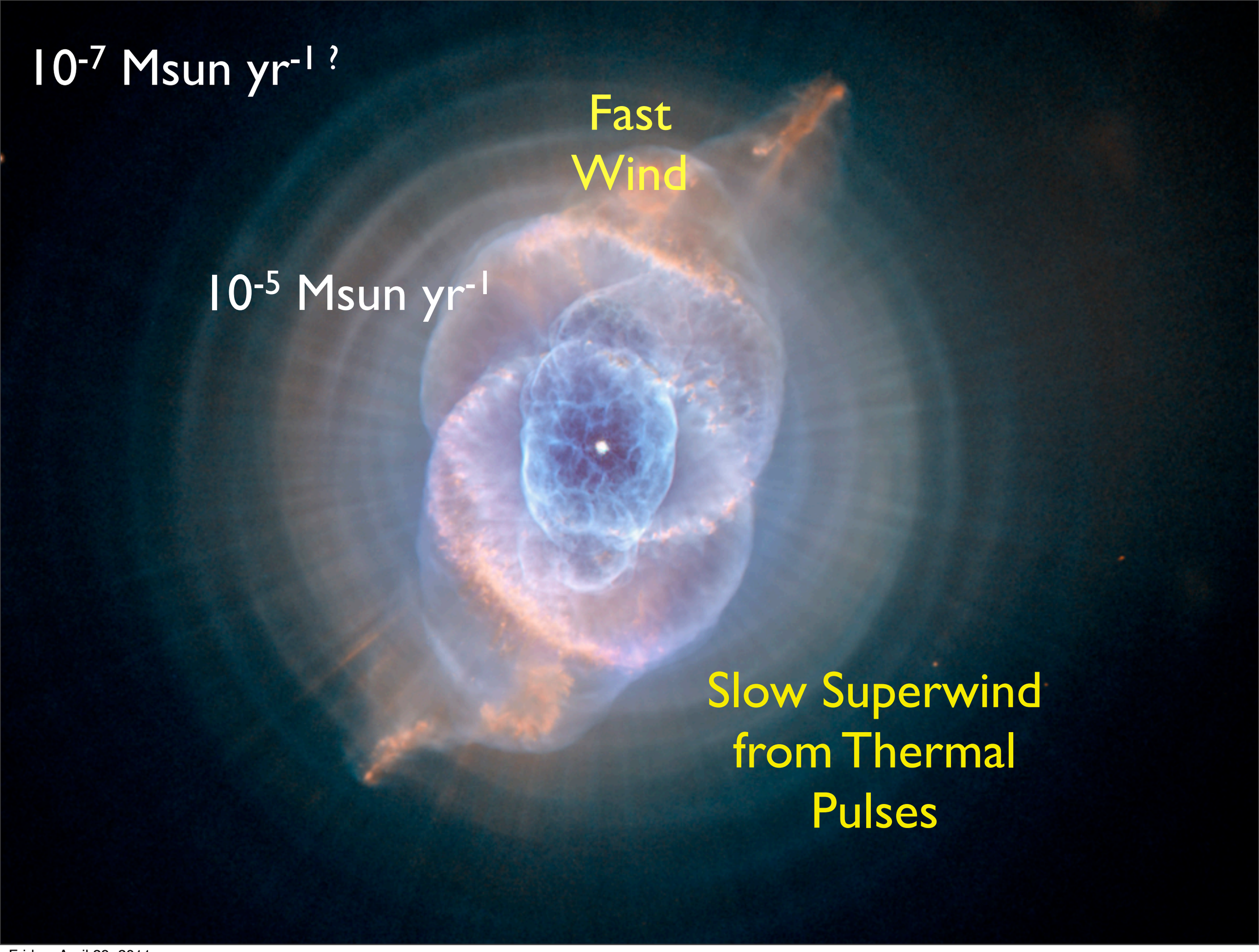
10^{-7} Msun yr^{-1} ?
Fast
Wind
10^{-5} Msun yr^{-1}
Slow Superwind
from Thermal
Pulses

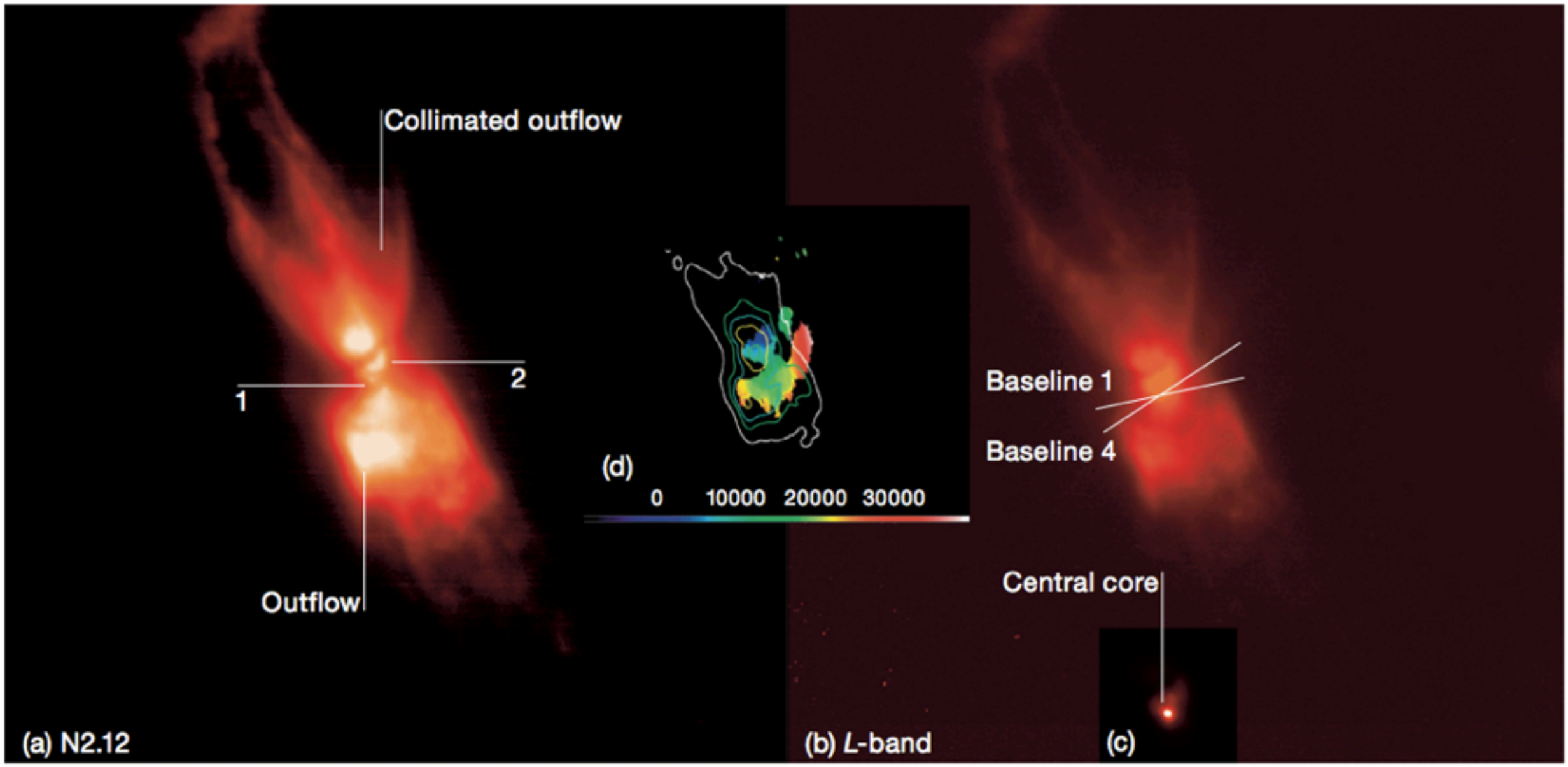

OH231.8+4.2 is the first source to show all components expected from the ISW model: an inner disc with size consistent with a circumbinary disc, a bipolar outflow, and a velocity field as predicted by a fast wind–slow wind interaction. The only missing ingredient is the putative binary companion. The very high opacity of the inner region may make this hard to find.

Figure 1: Composite of OH231.8+4.2. (a) 2.12 micron image. For scale, the banana-like structure (2) is 0.7 arcsec across. (b) *L*-band image: The position angles of the VLTI baselines are indicated. (c) A zoom on the bright core seen in the NACO *L*-band image. (d) OH maser velocities measured with MERLIN; the colour scale is in m/s.

Zijlstra 2006
ESO Messenger

547 nm
606 nm
658 nm
673 nm
953 nm

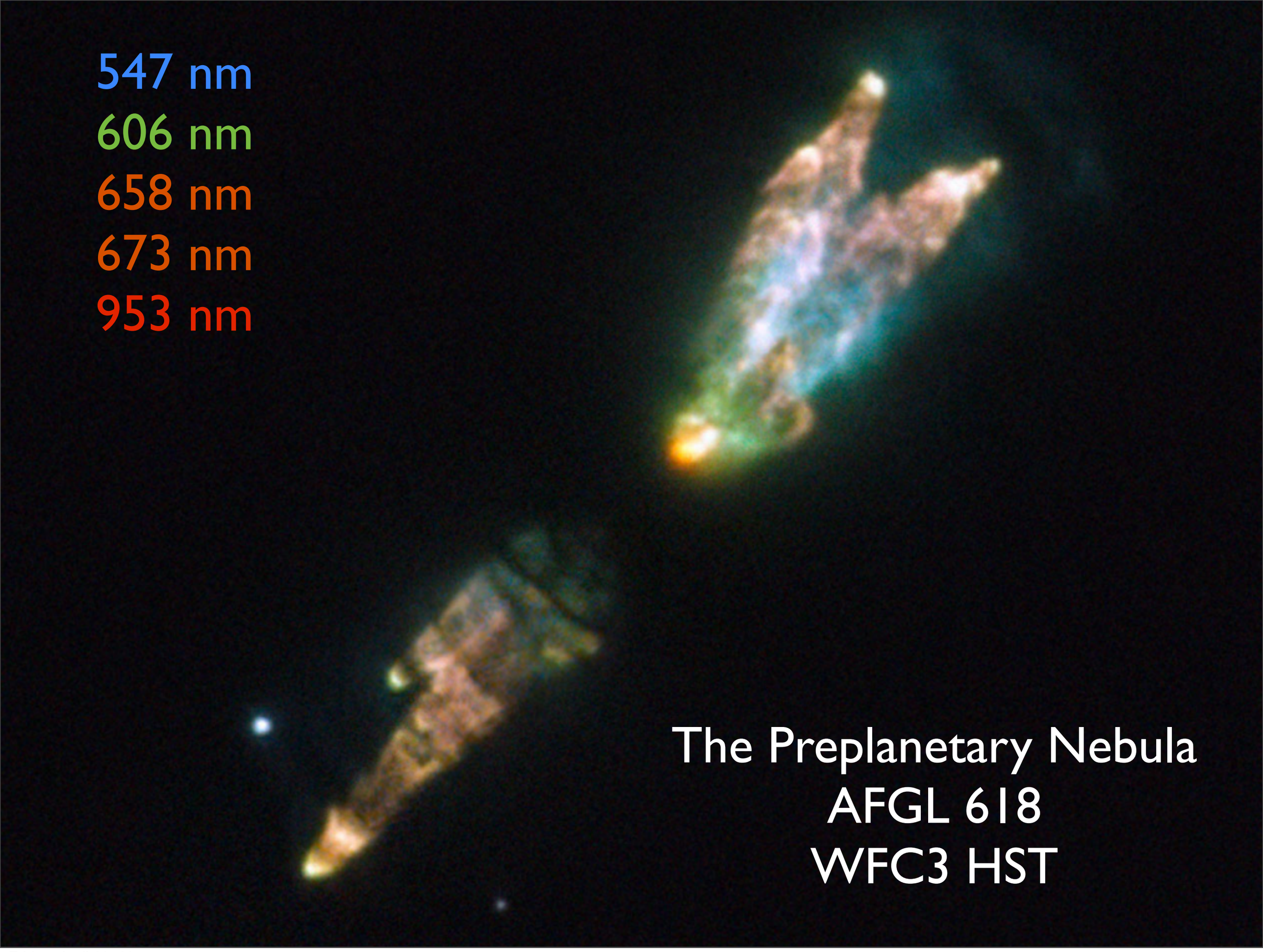

The Preplanetary Nebula
AFGL 618
WFC3 HST

Model for Preplanetary Nebula

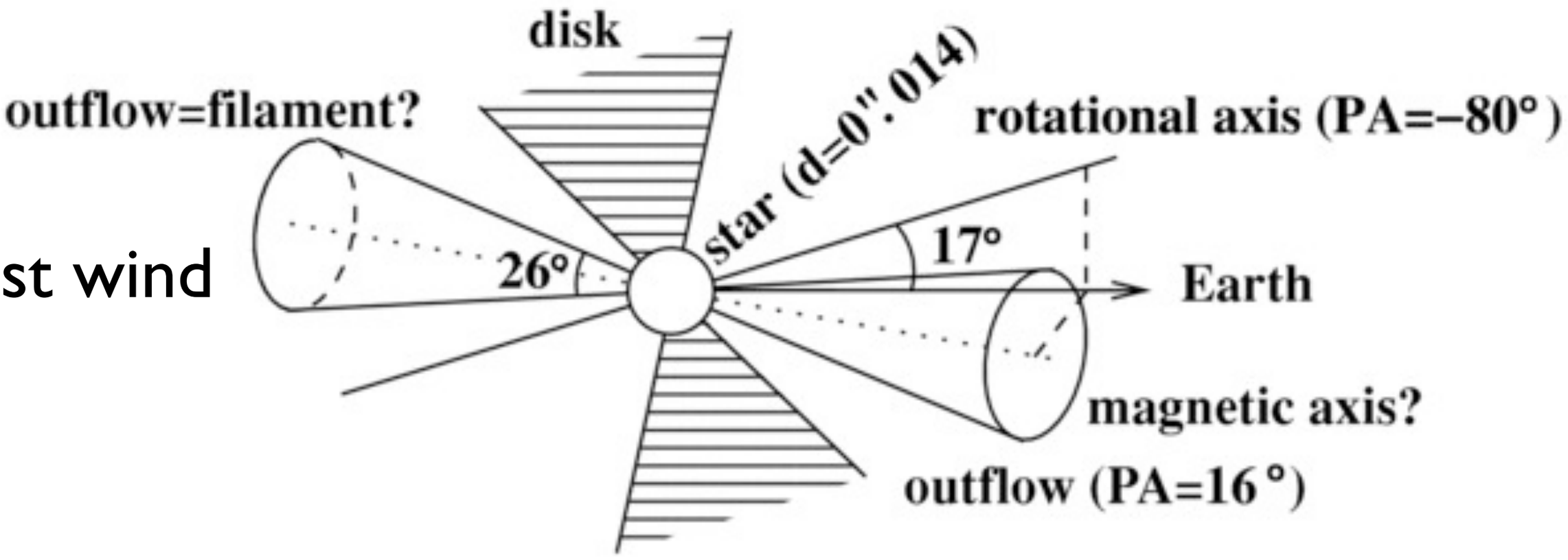

Fast wind

Slow superwind forming expanding disk?

Molecular Hydrogen Emission Toward AFGL 681

Cox et al. 2003

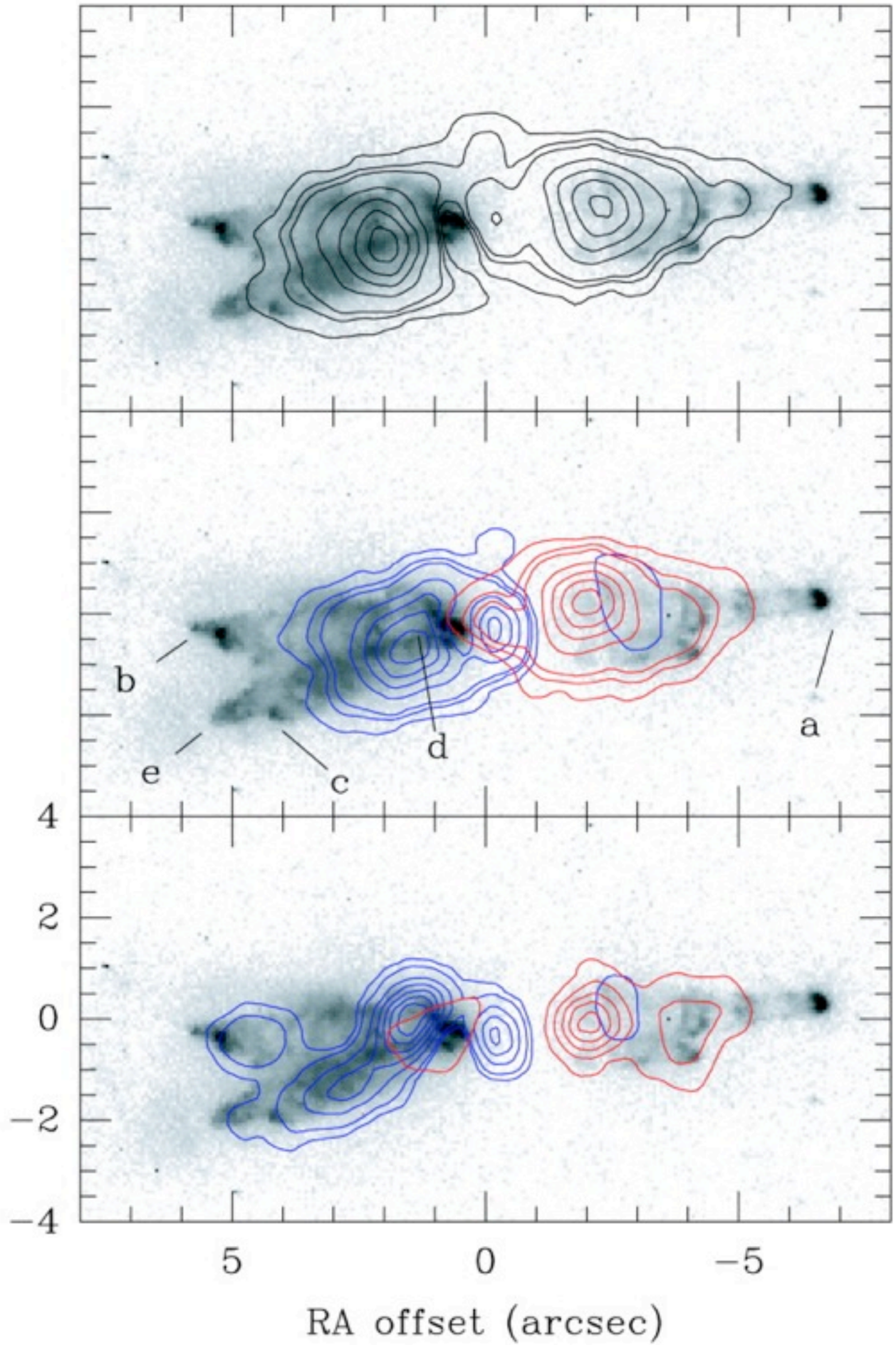

FIG. 3.—H_2 channel maps of AFGL 618 superposed on the *HST* Hα image. *Top*: Emission around the systemic velocity (−40 to −3 km s^{-1}). *Middle*: Blue and red intermediate velocities (−41 to −125 and −3 to 81 km s^{-1}). *Bottom*: Blue and red extreme velocities (−126 to −186 and 82 to 152 km s^{-1}). In the middle panel, the jets are labeled as in Trammell & Goodrich (2002). The contours are at 2, 6, and 10 to 100 by 20% of the peak intensity in each channel.

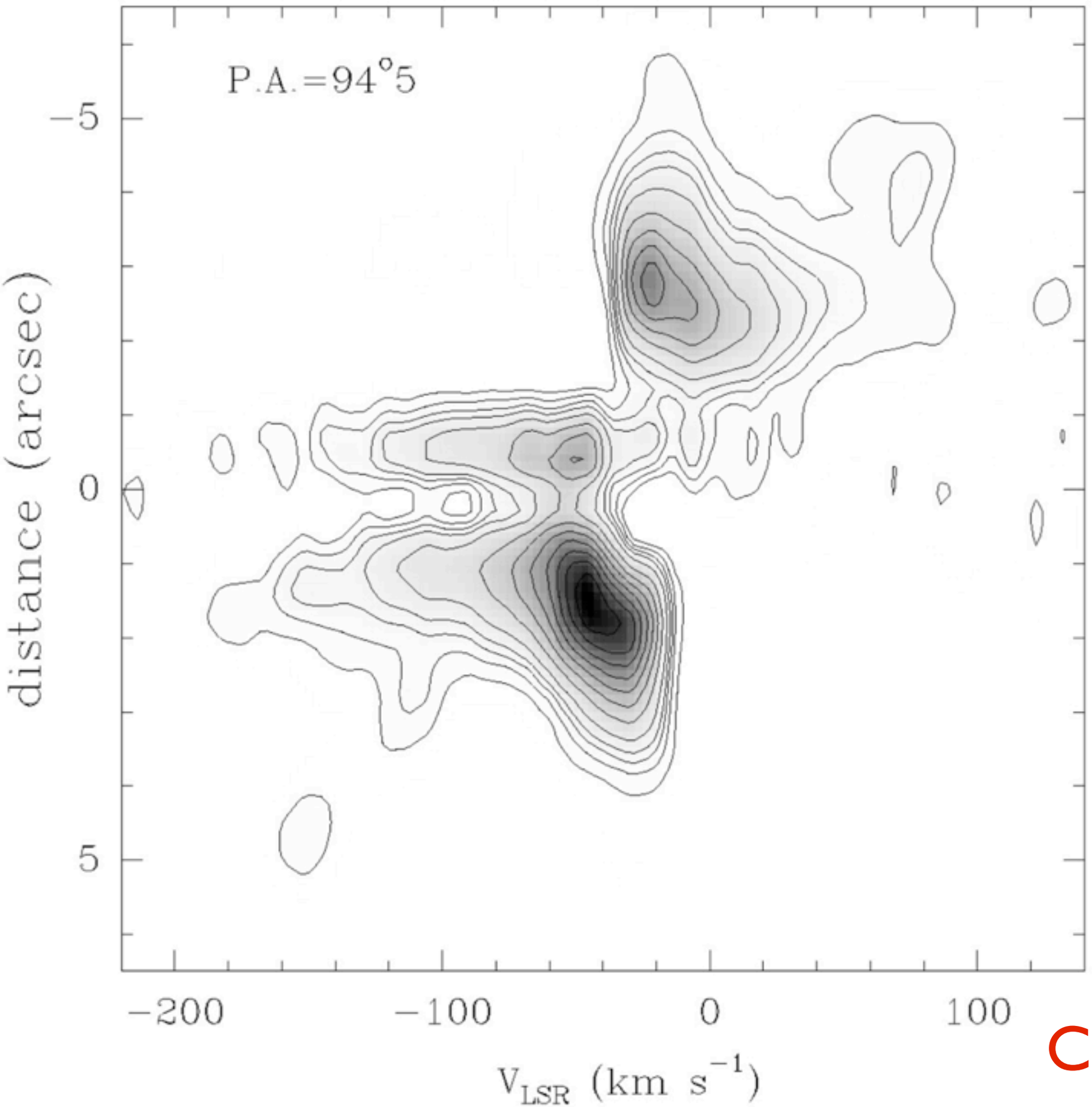

AFGL 618
H_2 Lines

Cox et al. 2003

The Pre-planetary Nebula AFGL 2688

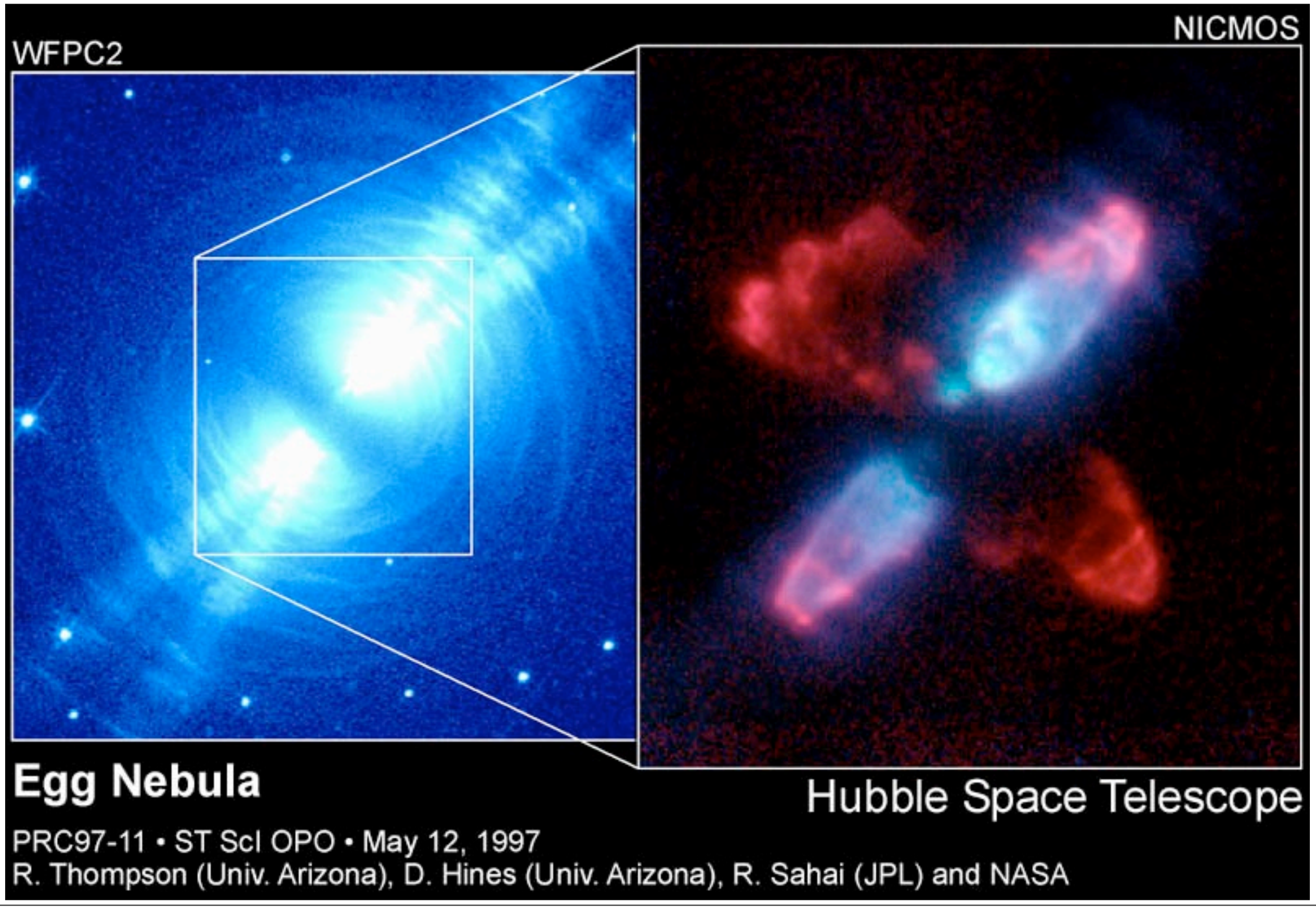

AFGL 2688

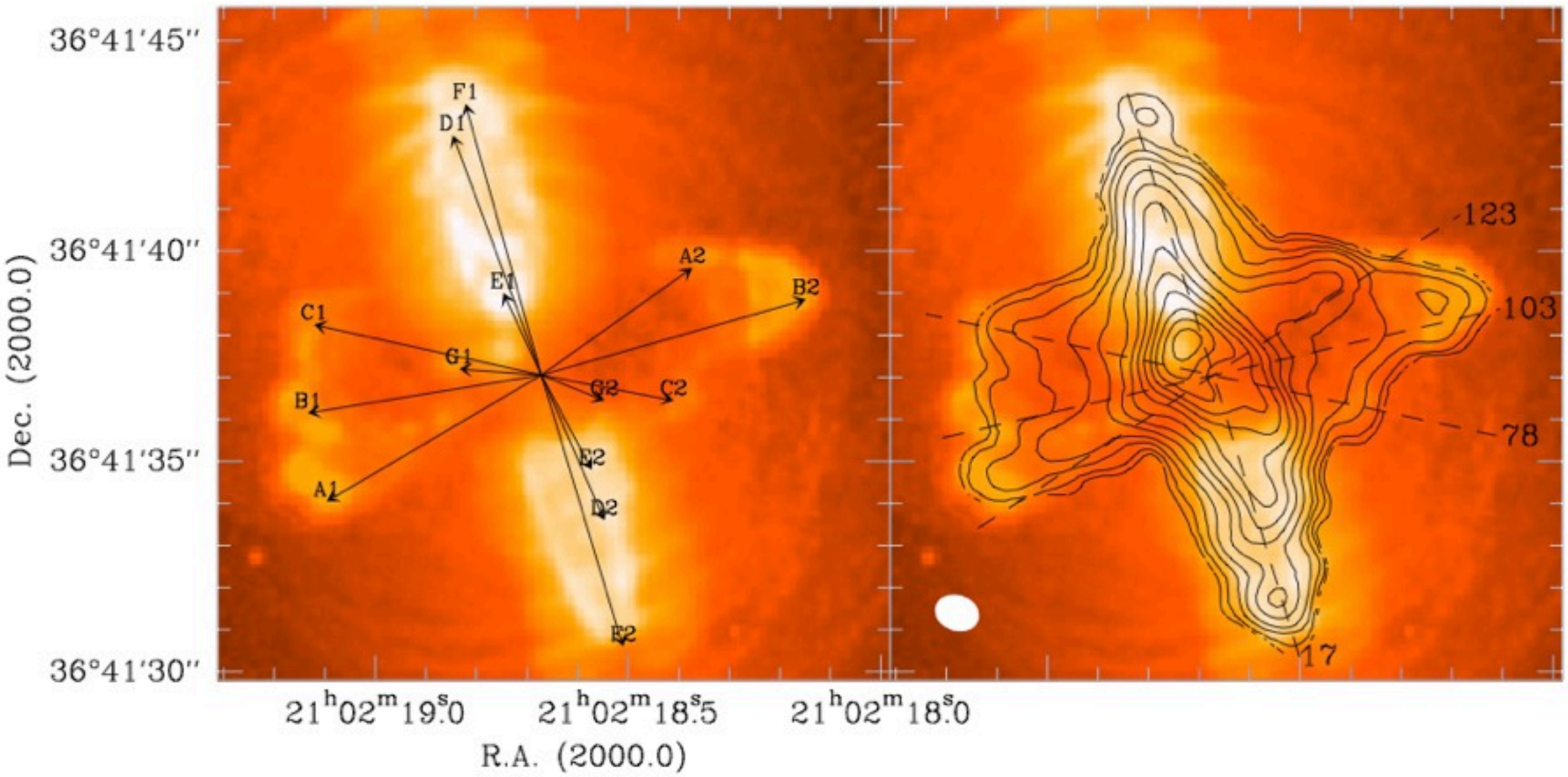

Fig. 2. The Plateau de Bure interferometer data compared to the H_2 1–0 S(1) line emission and nearby 2.15 μm continuum (in color) - from Sahai et al. (1998). The velocity integrated CO(2–1) emission is shown as contours (2, 4, 8, 12 to 72 by 6 Jy/beam) in the right panel, and the outflow axis are identified in the left panel (see also Fig. 1 and 3). The beam of the CO image is shown in the lower left corner of the right panel, with the locations of the position-velocity diagrams of Fig. 3

Cox et al. 2003

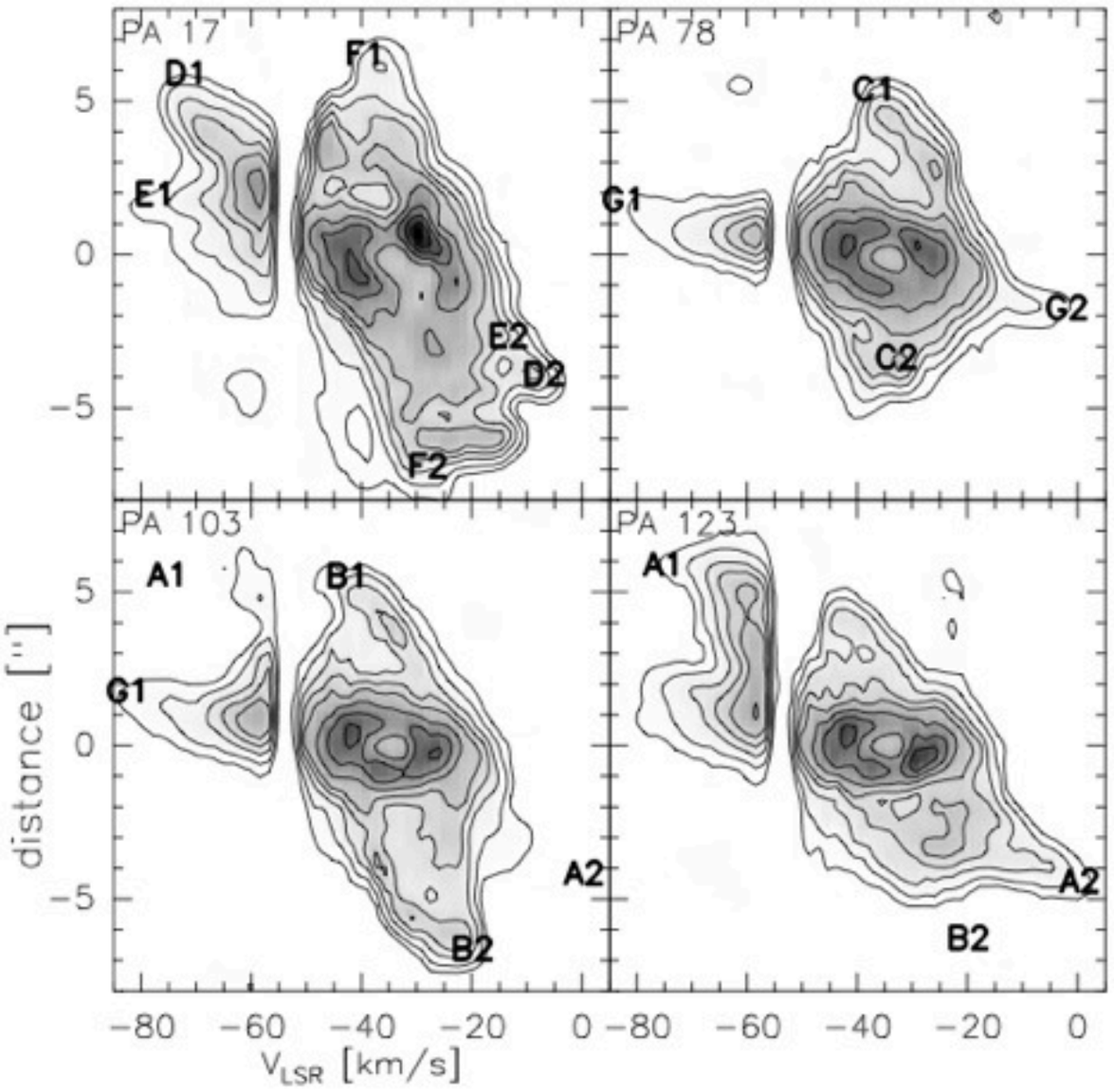

Fig. 3. Velocity-strip maps in the CO(2–1) line along the north-south bipolar outflow axis (P.A. 17°), and three east-west directions at P.A. of 78, 103, and 123° (see Fig. 2). The contours are 0.25, 0.5, 0.75, 1 to 2.6 by 0.4 Jy/beam. The extremities of the outflows are indicated.

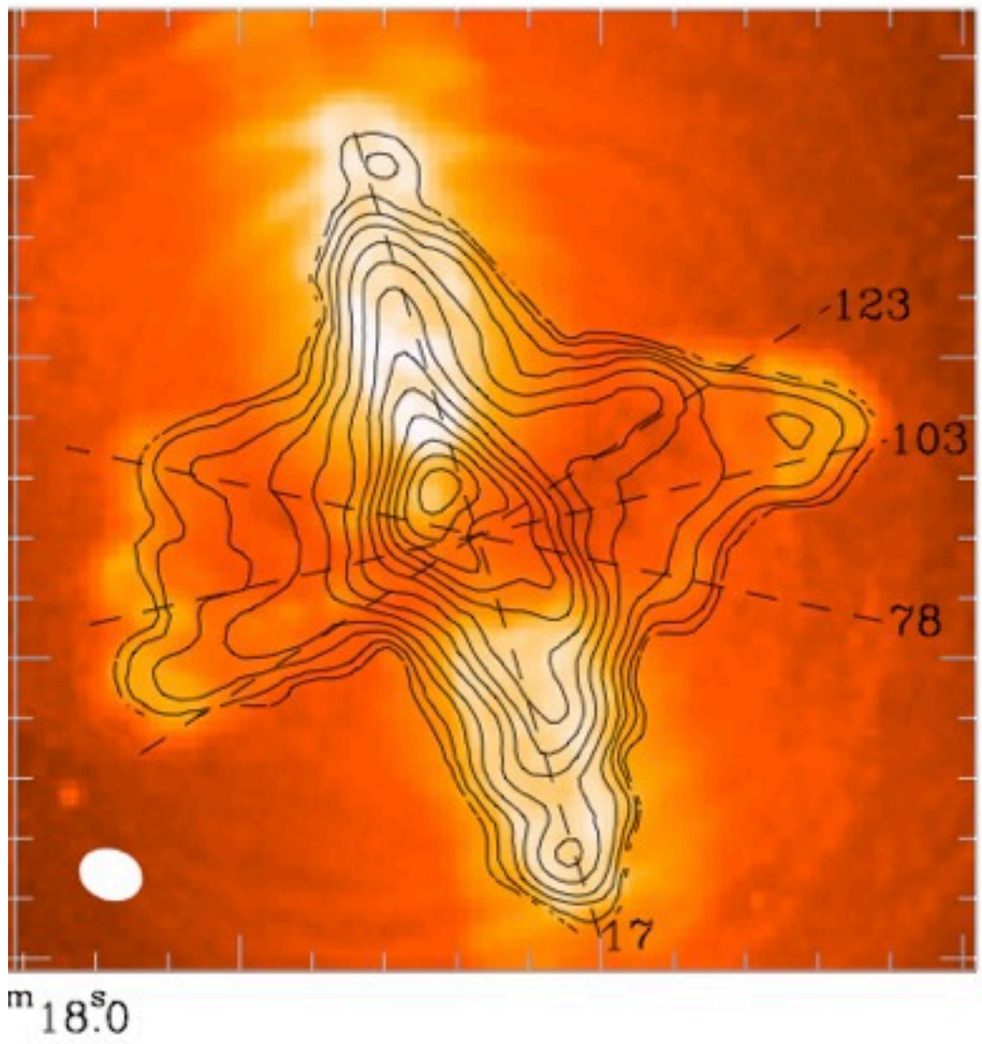

$^{m}18.^{s}0$

0 S(1) line emission and nearby 2.15 μm continuum (in color) - from as contours (2, 4, 8, 12 to 72 by 6 Jy/beam) in the right panel, and the am of the CO image is shown in the lower left corner of the right panel,

SEDs of Preplanetary Nebula

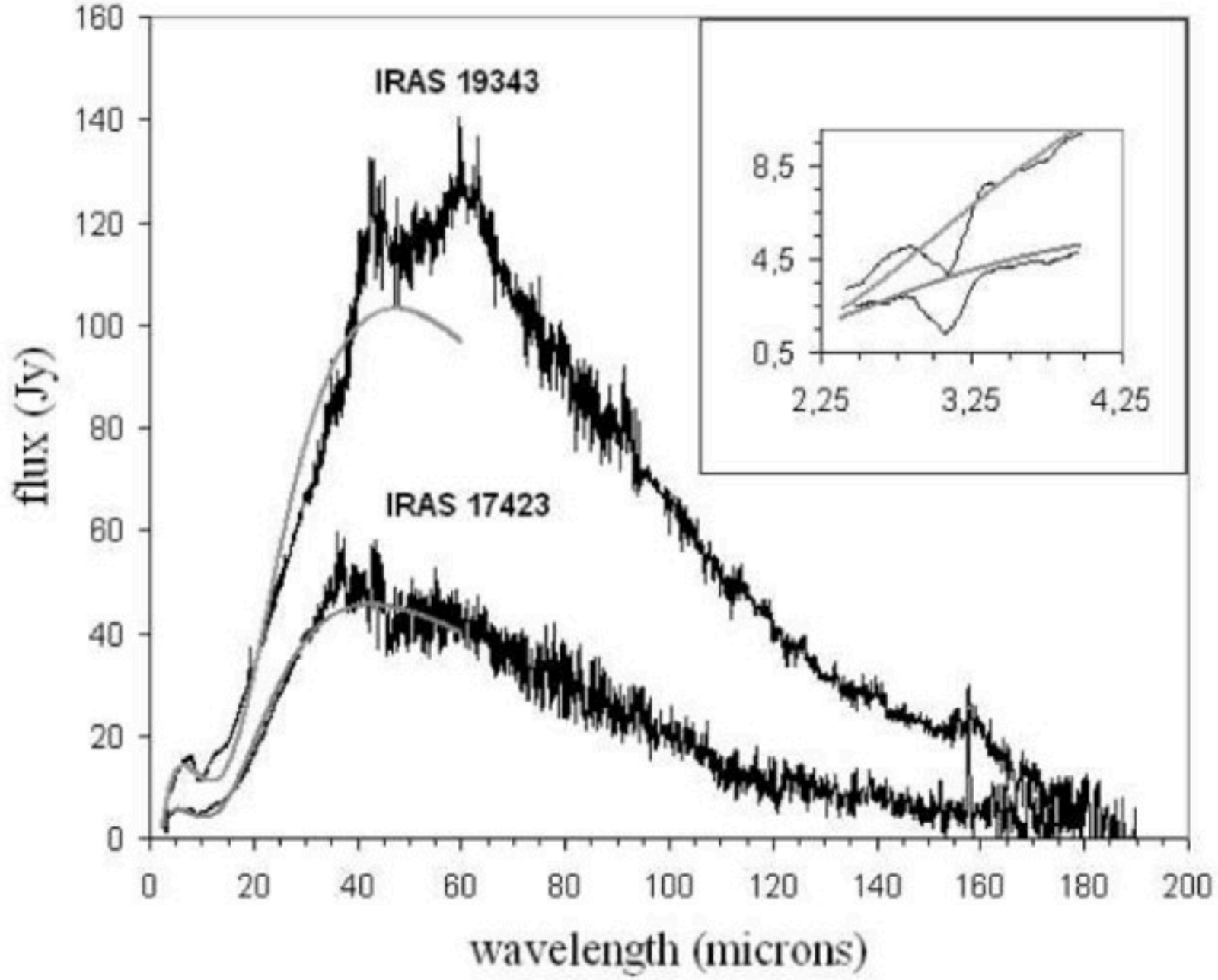

Fig. 2.— SED from ∼2 to 180 μm for IRAS 17423−1755 and IRAS 19343+2926. The SEDs were constructed by combining *Spitzer* and *ISO* data (see the text for details). The blackbody curves fitted to the spectra of both stars are also shown, corresponding to dust temperatures of 120 K and 965 K for IRAS 17423−1755, and 107 K and 800 K for IRAS 19343+2926. The spectral region around 3 μm is detailed in the small window.

Monteiga et al. 2011

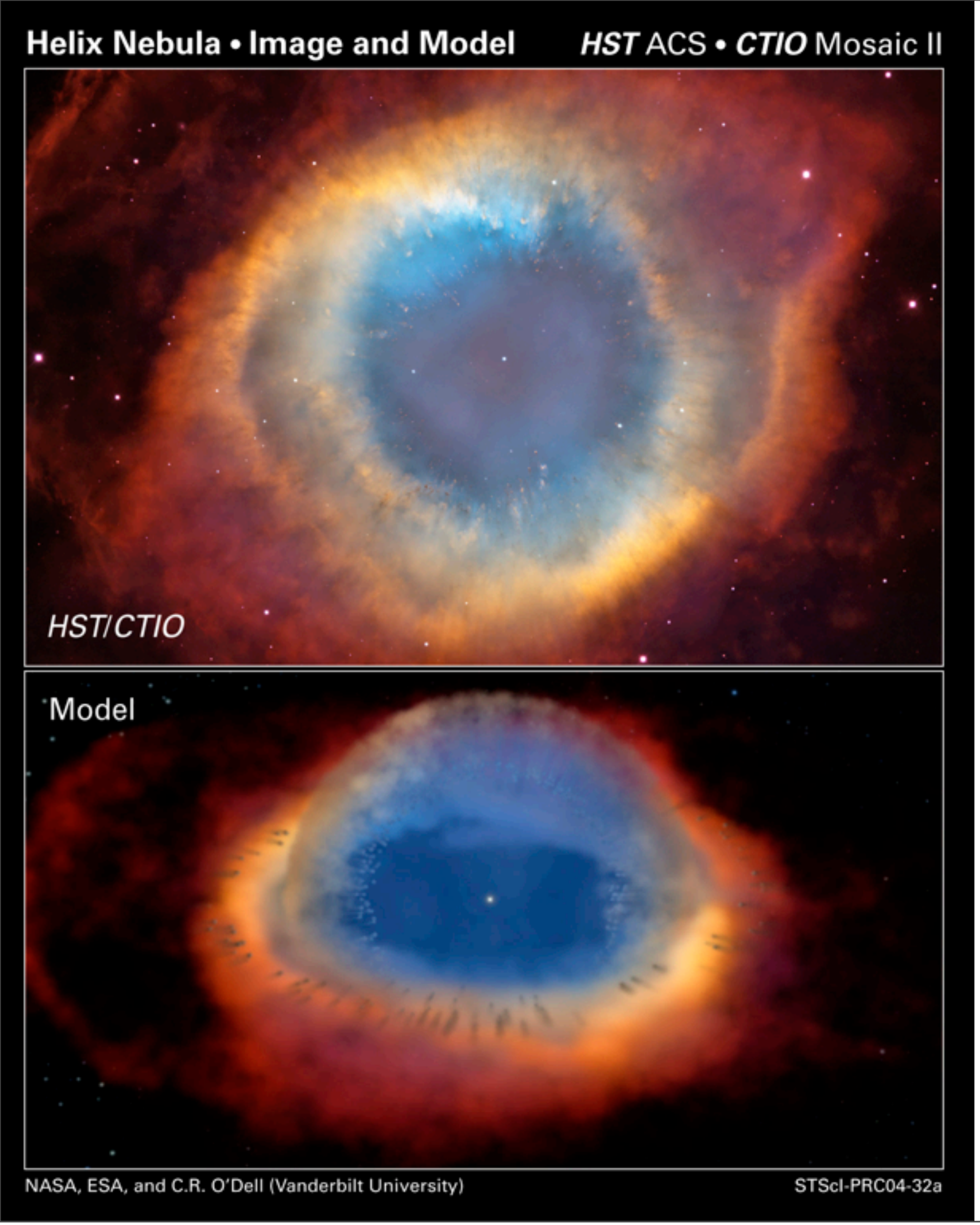

Eventually, the hot inner white dwarf is uncovered, creating a planetary nebula.

Do All Stars Undergo a Planetary Nebula Phase?

80% of Planetary Nebula are asymmetric.

Asymmetric planetary nebula may be best explained by close binaries.

Fast jets may require close binary systems to launch them (MHD launching).

Does this imply many stars do not form planetary nebula?

Could planets play a role?

De Marco 2011 and references therein

How do you get multiple jets from a binary?

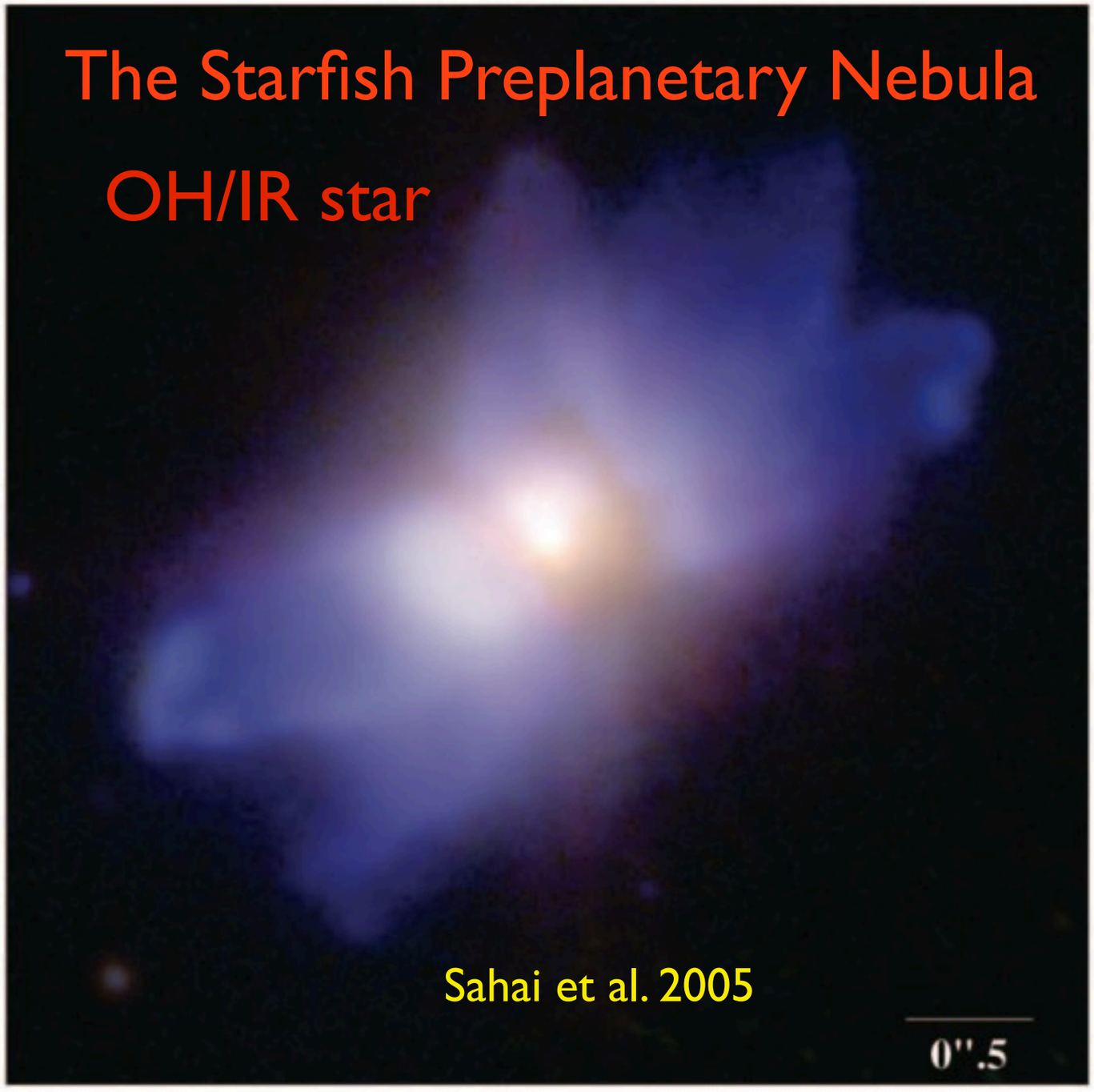

FIG. 5.—Color image (*log stretch*) of I19024, made by combining the F606W (*blue*), F110W (*green*), and F160W (*red*) images. The orientation of this image is identical to that in Figs. 1–4.

Summary

The AGB phases are characterized by thermal pulses occurring on a $10{,}000-100{,}000$ year period.

Mira variables are solar mass AGB stars showing pulsations on $300-1000$ day periods.

OH/IR stars are AGB stars showing OH masers in an expanding shells on strong IR emission due to dust formation in a shell. Most of their luminosity is radiated in the IR.

AGB stars show mass loss rates from 10^{-7} Msun yr^{-1} (wind) to 10^{-4} Msun yr^{-1} (superwind)

Planetary nebula are not circularly symmetric, but are elliptical and often show jets.

This asymmetry may be due to a faster, lower density wind, collimated by slower material ejected equatorial, magnetic fields, or possibly a binary (or planetary) companion.

Preplanetary nebula are an intermediate stage between AGB stars and planetary nebula

These sources still buried in a dense dust cloud (from dust formed in the wind), but show multiple, collimated, low density jets. Sometimes the jets are rotated up to 90 degrees from each other.